This is a preprint, the final version is subject to change, of the American Mineralogist (MSA)
Cite as Authors (Year) Title. American Mineralogist, in press.
(DOI will not work until issue is live.) DOI: http://dx.doi.org/10.2138/am-2015-5000 

REVISION 3 Manuscript #5000

# High-pressure equation of state and phase transition in $PbAl_2Si_2O_8$ feldspar

**Nadia Curetti, Piera Benna and Emiliano Bruno**

Dipartimento di Scienze della Terra, Via Valperga Caluso 35, I-10125 Torino, Italy

CrisDi Interdepartmental Center for Crystallography, Via P. Giuria 5, I-10125 Torino, Italy

*E-mail: piera.benna@unito.it

## Abstract

In situ high pressure X-ray diffraction study was performed on synthetic lead feldspar with composition $PbAl_2Si_2O_8$ (PbFsp). The crystals were synthesized from the melt and thermally treated at $T$ = 1150 °C for 12 h and at $T$ = 1000 °C for 70 h. At room condition the unit-cell parameters are $a$ = 8.3936(4), $b$ = 13.0498(7), $c$ = 14.3258(8) Å, β = 115.281(6) °, $V$ = 1418.9(1) Å$^3$; space group: $I2/c$; $Q_{od}$ = 0.7.

A single-crystal of lead feldspar was loaded in an ETH-type diamond anvil cell and unit-cell parameters were measured at 26 different pressures up to 8.4 GPa at room $T$. The evolution with $P$ of the unit-cell parameters and volume shows a strong discontinuity between 7.7 and 8.2 GPa indicating a first order-phase transition. The discontinuous character of the transition is especially noticeable in the behavior of the β angle, which decreases from 114.83 to 114.03 °, and in the $b$ parameter, which reduces from 12.746 to 12.567 Å.

In the $P$ range 0.0001 - 7.72 GPa the trend shown by the axial compressibility ($\beta_a > \beta_c > \beta_b$) is similar to that observed in the previous H$P$ powder diffraction study, performed on lead feldspar using high-brilliance synchrotron radiation up to 7.1 GPa. In the $P$ range 0.0001 - 4.27 GPa at room $T$, the $P$-$V$ data of the $I2/c$ lead feldspar were fitted with a second-order Birch-Murnaghan EoS. The parameters obtained are: $V_0$ = 1422.2 (1) Å$^3$ and $K_{T0}$ = 76.4(9) GPa. At $P$ > 4.27 GPa, the volume values deflect from the BM2 curve and show a volume softening, precursor of the reported H$P$ phase transition. A volume softening was recently observed in strontium feldspar (SrFsp) above 4.2 GPa.

A second crystal of PbFsp was loaded in the DAC cell and in situ high pressure X-ray diffraction intensities were measured at $P$ = 0.0001, 2.4, 3.1, 5.4, 6.0, 7.2, 8.4 and 9.7 GPa. The appearance of *c* and *d*-type reflections at 8.4 GPa, the analysis of the systematic absence and the structural refinements indicate the H$P$ first-order transformation as an $I2/c$ - $P2_1/c$ phase transition. Structural results show that the main variations with compression in lead feldspar are in Pb-O bond lengths and in T-O-T bond angles, while T-O distances and O-T-O angles does not change meaningfully, indicating that the Si,Al tetrahedra behave with pressure as a rigid body. Changes observed in the compressional behaviour of the structure between 3 and 5 GPa could explain the softening observed at $P$ > 4 GPa in the volume compressibility.
The results obtained in the present work allow comparing the pressures of the H$P$ $I2/c$ - $P2_1/c$ phase transition occurring in lead feldspar with those observed in alkaline-earth feldspars.

**Keywords**: Crystal structure, high-pressure studies, lead feldspar, equation of state, phase transition.

## Introduction

Several study were performed on natural and synthetic feldspars in order to investigate their equations of state (EoS) and symmetry changes with pressure; however, taking into account the complexity of their potential chemical and structural arrangements, the number of high quality data available in literature remains still limited. In a review on the behavior of feldspars at high-pressure conditions, Angel (1994) and Ross (2000) observed that the tetrahedra of the framework behave like almost a rigid body and the major compressional mechanism is the T-O-T bond bending. The degree of Al,Si order influences the H*P* elastic behavior of feldspars and, in particular, an increase of Al,Si disorder results in a small decrease in bulk modulus (Angel et al. 1988; Angel 1994; Downs et al. 1994; Allan and Angel 1997; Benusa et al. 2005; Sochalski-Kolbus et al. 2010; Curetti et al. 2011b).

In feldspars with Al:Si ratio equal to 1:1, the symmetry at room condition is determined by the non-tetrahedral M cation: triclinic $P\bar{1}$ (or $I\bar{1}$) space group is observed when the M-site is occupied by Ca (anorthite, $CaAl_2Si_2O_8$, An, Megaw et al. 1962), monoclinic $I2/c$ symmetry when the M-site is occupied by a larger cation as Sr, Pb, Ba (strontium feldspar, $SrAl_2Si_2O_8$, SrFsp, Chiari et al. 1975; lead feldspar, $PbAl_2Si_2O_8$, PbFsp, Bruno and Facchinelli 1972; $BaAl_2Si_2O_8$, celsian, Newman and Megaw 1960). Along the anorthite - strontium feldspar (An-SrFsp) join at ambient conditions, the structure of feldspars changes with composition from $P\bar{1}$ to $I2/c$, through an intermediate $I\bar{1}$ structure. The $P\bar{1}$ - $I\bar{1}$ phase transition occurs near $An_{50}SrFsp_{50}$ composition (Phillips et al. 1997; Tribaudino et al. 2000, 2005) and the

$I\bar{1}$ - $I2/c$ zone-centre displacive ferroelastic transition, strongly affected by different Al,Si order (Tribaudino et al. 1993, 2009), was observed near $An_{10}SrFsp_{90}$ in ordered feldspars (Bambauer and Nager 1981; McGuinn and Redfern 1994) and near $An_{20}SrFsp_{80}$ in more disordered samples (Bruno and Gazzoni 1968). The same $I\bar{1}$ - $I2/c$ transition can be observed with increasing temperature in Sr-rich feldspars that are triclinic at room temperature and the temperature of the transition changes with the degree of order at constant composition (Bruno and Gazzoni 1968; Nager et al. 1969; Tribaudino et al. 1993; McGuinn and Redfern 1997; Benna and Bruno 2003). Regard lead feldspar, Benna et al. (1996) synthesized both disordered ($C2/m$ space group, absence of *b*- type superlattice reflections, macroscopic order parameter $Q_{od}$ = 0) and ordered ($I2/c$ space group, $Q_{od}$ = 0.9) configurations. At room temperature, in the Pb-rich region of the anorthite - lead feldspar (An-PbFsp) join, the $I\bar{1}$ - $I2/c$ phase transition occurs near $An_{10}PbFsp_{90}$ composition (Benna et al. 2000).

The volume compressibility of the Al:Si = 1:1 feldspars was frequently determined in a limited pressure range because these crystals experience phase transitions at low pressures. Angel et al. (1988) studied the compressibility of anorthite and found a reversible first-order $P\bar{1}$ to $I\bar{1}$ phase transition between 2.6 and 3.0 GPa, by means of in situ H*P* investigations. An increase in the pressure of the $P\bar{1}$ - $I\bar{1}$ transition with increasing disorder, together with a trend from first-order character to a more continuous transition, was observed by Angel (1992). Using in situ H*P* Raman spectroscopy, Daniel et al. (1995) observed in anorthite a further reversible transition at about 10 GPa, associated with drastic changes in the position of the

vibrational modes, but the newly formed phase was not identified. In the $An_{20}SrFsp_{80}$ feldspar, triclinic at room temperature, Nestola et al. (2004) observed a first-order transformation from $I\bar{1}$ to $I2/c$ at $P \sim 4.3$ GPa, and a further transition, strongly first-order, from monoclinic $I2/c$ to monoclinic-II phase at $P \sim 7.3$ GPa. This second transformation was defined as an $I2/c$ - $P2_1/c$ transition by Benna et al. (2007) and the $P2_1/c$ configuration was studied by H$P$ in situ single-crystal XRD. The volume bulk modulus of $P\bar{1}$ anorthite is 83.3 GPa (Hackwell and Angel 1992) and a value of around 82.5 GPa has been extrapolated for $I\bar{1}$ anorthite from the compression behavior of plagioclases (Angel 2004). Since the volume bulk modulus of the triclinic $An_{20}SrFsp_{80}$ is 88.7 GPa, the substitution of 80% of $SrAl_2Si_2O_8$ component into the anorthite structure causes a slight increase in the bulk modulus (Pandolfo et al. 2011). In recent studies, Pandolfo et al. (2011) and Mrosko et al. (2011), with completely different analytical techniques (in situ single-crystal XRD and mid/far micro-FTIR spectroscopy), found in strontium feldspar a similar first-order $I2/c$ to $P2_1/c$ transition at $P$ = 6.6 and 6.5 GPa, respectively. The bulk modulus of strontium feldspar is 90 GPa up to 3.7 GPa, with a volume softening for $P$ > 4.2 GPa. In a preliminary study on H$P$ behavior of barium feldspar, Curetti et al. (2011a) observed a similar phase transition between 5.5 and 5.9 GPa in natural celsian.

In conclusion, the pressure induced phase transitions until now known in Ca-Sr-Ba feldspars are: the triclinic $P\bar{1}$ - $I\bar{1}$ (anorthite), the triclinic $I\bar{1}$ - monoclinic $I2/c$ ($An_{20}SrFsp_{80}$) and the monoclinic $I2/c$ - $P2_1/c$ transition (strontium feldspar, $An_{20}SrFsp_{80}$, celsian).

In situ H$P$ powder diffraction study was performed on lead feldspar by

Tribaudino et al. (1999), using high-brilliance synchrotron radiation. Two samples, with $Q_{od}$ = 0.68 and 0.76, were compressed up to 11 GPa. Until $P$ = 7.1 GPa the only phase present was lead feldspar. In the range 7.1 - 9.4 GPa sudden changes in the position of the reflections suggest the transformation of lead feldspar to a new phase (probably feldspar-like), but the powder diffraction data do not provide clear evidence of the transition.

The aim of this work is to study at H$P$ conditions in situ the synthetic partially ordered lead feldspar ($Q_{od}$ = 0.7) by means of the single-crystal X-ray diffraction technique in order to investigate the high-pressure behavior of lead feldspar and to detail the possible presence of phase transitions.

## Experimental methods

The lead feldspar studied in this work, with composition $PbAl_2Si_2O_8$, was synthesized from melt as in Benna et al. (1996). The sample was then annealed at $T$ = 1150 °C for 12 h and further annealed at $T$ = 1000 °C for 70 h in an electric furnace (SiC resistance, Pt-PtRh 10% thermocouple), using unsealed Pt tubes. X-ray powder diffraction revealed that lead feldspar was the only crystalline phase.

A single crystal of lead feldspar of size 150 x 75 x 50 $\mu m^3$ was selected on the base of its optical features and its preliminary characterization was performed using a Gemini R Ultra single-crystal X-ray diffractometer equipped with a Ruby CCD detector, using monochromatic Mo$K\alpha$ radiation and the tube operating at 50 kV and 40 mA (CrisDi Interdepartmental Center, University of Torino). A total of 202 frames were collected (frame width 1°, exposure time 9.1 s, sample-detector distance 55 mm) covering the

whole accessible reciprocal space; 4312 reflections were measured, of with 2274 unique. The 171.36.24 version of CrysAlysPro software (Agilent Technologies) was used to integrate the intensity data and for analytical absorption and Lorentz-polarization correction. The data collection shows only *a* (*h* + *k* = even, *l* = even) and *b*–type (*h* + *k* = odd, *l* = odd) reflections, confirming the *I*2/c space group as in Benna et al. (1996). With $F_O \geq 2\sigma(F_O)$ the number of *a* and *b* reflections observed is 1123 and 873, respectively. Unit-cell parameters at room conditions are *a* = 8.3936(4), *b* = 13.0498(7), *c* = 14.3258(8) Å, β = 115.281(6) °, *V* = 1418.9(1) Å$^3$. The structural data were refined starting from the fractional coordinates of lead feldspar reported in Benna et al. (1996) and using the neutral atomic scattering factor of the Pb, Si, Al and O. The M-site was refined according to the 'Pb split-atom model' (Tribaudino et al. 1998). The anisotropic refinement of 128 parameters converges at *R* = 4.96% for 1679 reflections with $F_O \geq 4\sigma(F_O)$ and *R* = 7.15% for all data. Structural details were refined using SHELX-97 package (Sheldrick 2008). The Pb coordination polyhedron shows a significant distortion, probably related to the lone-pairs effect (Benna et al. 1996; Tribaudino et al. 1998). The macroscopic order parameter $Q_{od}$, calculated from <T-O> bond lengths following Angel et al. (1990), is equal to 0.7 and indicates a partially ordered Al,Si distribution. The structural results obtained at room conditions agree with those reported by Tribaudino et al. (1998) for the $PbF_L64h$ sample, annealed at *T* = 1000 °C for 64 h, with a similar value of $Q_{od}$.

Afterwards the room *T* characterization, the sample was loaded in an ETH-type diamond anvil cell (DAC, hereafter) (Miletich et al. 2000). A foil of T301 steel 250 μm

thick was used as a gasket to hold the crystal and it was pre-indented to 110 μm before drilling a hole by spark erosion (Ø 250 μm). A 16 : 3 : 1 mixture of methanol : ethanol : water was used as hydrostatic pressure-transmitting medium. The internal pressure was checked with Horiba-Jomin Micro-Raman spectrometer (Scansetti Interdepartmental Centre, University of Torino), by the shift of the fluorescence lines of five rubies (Ø 15 μm) scattered in the "hole" of the DAC. The uncertainty on *P* was estimated to be about 0.1 GPa (Mao et al. 1986). The unit-cell parameters were determined at room *T* in the *P* range 0.0001 - 8.4 GPa from the setting angles of 20-35 reflections centered in eight position (King and Finger 1979; Angel et al. 2000), using a Siemens P4 four circles X-ray diffractometer equipped with a point detector (Mo*K*α radiation; Department of Earth Sciences, University of Torino) and with the SINGLE Control Program software (Angel and Finger 2011). The unit-cell parameters were measured at overall 26 different pressures, in both increasing- and decreasing- *P*, in order to check the reversal behavior of the sample. Unit-cell parameters are reported in Table 1. Measurements made on compression and decompression confirmed that the cell parameter changes are reversible with no pressure hysteresis.

Another crystal of lead feldspar of the same synthesis was selected (size 160 x 80 x 60 $\mu m^3$) and loaded in the DAC cell in order to investigate the structural changes with increasing pressure. Unit-cell parameters at room conditions are $a$ = 8.3941(4), $b$ = 13.022(11), $c$ = 14.3153(7) Å, β = 115.253(6)°, $V$ = 1415(1) $Å^3$. Single crystal diffraction intensities were collected with Gemini R Ultra X-ray diffractometer (see before) at *P* = 0.0001, 2.4, 3.1, 5.4, 6.0, 7.2, 8.4 and 9.7 GPa (16 runs with a total of 2116 frames, frame width 0.2°, exposure time 50 s, sample-detector distance 82 mm).

Integrated intensities were corrected for the absorption of the DAC cell and for the gasket shadow using ABSORB-7 software (Angel and Gonzalez-Platas 2013). Structural details were refined using SHELX-97 package (Sheldrick 2008). The measurements at room pressure and at $P$ = 2.4, 3.1, 5.4, 6.0, 7.2 GPa showed only $a$ and $b$-type reflections confirming the $I2/c$ space group. At $P$ = 8.4 and 9.7 GPa, the data collection also showed the presence of $c$ ($h + k$ = even, $l$ = odd) and $d$-type reflections ($h + k$ = odd, $l$ = even) indicating a primitive lattice; reflection extinctions were accurately investigate and since reflections $h0l$ and $00l$ with $l$ = even only were observed (unfortunately, because of the shape and orientation of the crystal in the DAC, it has not been possible to measure $0k0$ diffractions in order to verify the presence of a screw axis along the $b$ direction), the analysis of the systematic absences confirms the $P2_1/c$ symmetry at $P$ = 8.4 and 9.7 GPa. In the $P2_1/c$ refinements all the atoms of $I2/c$ symmetry were splitted in two non-equivalent sites taking into account the change of origin by ¼, ¼, ¼ in the $P2_1/c$ space group. For all the refinements, anisotropic displacement parameters were introduced only for extra-framework Pb cations. Unit-cell parameters and refinements details are reported in Table 2. Fractional atomic coordinates and displacement parameters are shown in Tables 3 and 4. Pb-O interatomic distances and T-O-T bond angles are listed in Tables 5 and 6 respectively.

## Results and discussion

### Lattice deformation

The unit-cell parameters of lead feldspar up to $P$ = 8.35 GPa are reported in Table 1 and the evolutions of the unit-cell parameters and volume with pressure are shown in Fig. 1 and Fig. 2, respectively. A strong discontinuity is visible at about 8 GPa

indicating a first-order phase transition at high pressure.

In the *P* range 0.0001 - 7.72 GPa the *a*, *b* and *c* parameters (Fig. 1) decrease with increasing pressure with a subtle change in the trend for *P* higher than 4 GPa. The linear parameters show a negative axial variation by 4.3, 2.4 and 3.6% respectively, to the maximum pressure considered (*P* = 7.72 GPa). The axial compressibilities are $\beta a$ = 5.57, $\beta b$ = 3.12, $\beta c$ = 4.72 $\times 10^{-3}$ $GPa^{-1}$ (with $\beta = -(d - d_0)/d_0 \times 1/P$ where *d* is a unit-cell parameter) and show the typical trend previously observed in feldspars: $\beta a > \beta c > \beta b$ (Angel et al. 1988). The comparison of the three linear compressibilities shows an axial anisotropy ($\Delta a/a_0 : \Delta b/b_0 : \Delta c/c_0$ =1.8:1:1.5) higher than in *I*2/*c* $An_{20}SrFsp_{80}$ and $SrFsp_{100}$ feldspars (1.2:1:1.2, Nestola et al. 2004; Pandolfo et al. 2011) and slightly higher than in anorthite (1.6:1:1.5, Angel et al. 1988), but lower than in overall alkali feldspars studied at H*P*, as anorthoclase (2.4:1:1.4, Nestola et al. 2008), analbite (2.4:1:1.2, Curetti et al. 2011b), low albite (3.3:1:1.3, Benusa et al. 2005), sanidine (5.2:1:2.4, Angel et al. 1988) and microcline (8.3:1:4.1, Allan and Angel 1997).
The lattice β angle weakly increases up to about 1.8 GPa reaching the maximum value of 115.32 ° and then as much weakly decreases for higher pressures (Table 1, Fig. 1). A similar trend in β angle was observed by Tribaudino et al. (1999) in lead feldspar up to 7.1 GPa in a H*P* powder diffraction study. Considering all the other feldspars till now examined at H*P*, the β angle decreases in anorthite, celsian (Curetti et al. 2011a), $SrFsp_{100}$ and $An_{20}SrFsp_{80}$ feldspars, while it increases in alkali feldspars with a plateau effect (Allan and Angel 1997; Nestola et al. 2008).

The strain induced in lead feldspar by increasing pressure up to 7.72 GPa has been evaluated (Win_Strain4 program, Angel software 2011) in order to compare the

magnitudes and the orientations of the principal axes of the strain ellipsoid with those observed in the other feldspars compressed at H*P* (Angel et al. 1988; Angel 1994). In lead feldspar the highest deformation occurs on the 010 plane, with the main axis $\boldsymbol{\varepsilon_1}$ only slightly more compressible than the others (44% of the total strain), similarly to strontium feldspar (42%, Pandolfo et al. 2011). The strain ellipsoids in alkali feldspars and in anorthite are significantly more anisotropic and their orientation are quite different: in alkali feldspars some 55-65% of the volume compression is accommodated by the linear compression close to **a*** (Angel et al. 1988; Allan and Angel 1997; Nestola et al. 2008; Curetti et al. 2011b) and in anorthite the maximum compression occurs close to the 001 plane with 70% of the total strain along $\boldsymbol{\varepsilon_1}$ axis (Angel 1994).

**Equation of state**

Fig. 2 shows that in the pressure range 0.0001- 7.72 GPa in $I2/c$ lead feldspar at $P$ > 4.27 GPa there is some evidence for a change in the compressional behavior of the unit-cell volume with pressure. So we have used a second-order Birch-Murnaghan Equation of State (BM2-EoS) to fit the $P$-$V$ data only up to 4.27 GPa, using the EosFit7c software (Angel et al. 2014) with the resulting EoS coefficients: $V_0$ = 1422.2(1) Å$^3$, $K_{T0}$ = 76.4(9) GPa. An attempt to fit the $P$-$V$ data to a BM3-EoS or some other EoS in the $P$ range 0.0001 - 4.27 GPa did not provide any reliable results, probably because of the too small a pressure range. Fitting the $P$-$V$ data to a BM2-EoS in the $P$ range 4.79 - 7.72 GPa gives a lower bulk modulus, 63.2(2.3) GPa, confirming the anomalous volume behaviour at $P$ > 4.27 GPa. When our $P$-$V$ data are reformulated as a normalized

pressure - finite strain plot ($F_E$ - $f_E$ plot, Angel 2000), the values in the *P* range 0.0001 - 4.27 GPa lie on an horizontal line of constant $F_E$ (indicating $K' = 4$) (Fig. 3), confirming that the data are adequately described by a BM2-EoS. The anomalous behaviour of the volume values (Fig. 2), that deflect from the BM2 curve (solid line) at $P > 4.27$ GPa, could be defined as a volume softening. This softening, quite evident near 6 GPa and over, could be a precursor of the H*P* first-order phase transition observed at about 8 GPa. In strontium feldspar too, a volume softening within the $I2/c$ symmetry above 4.2 GPa was recently observed by Pandolfo et al. (2011).

The volume bulk modulus of lead feldspar, 76.4(9) GPa, is clearly lower than that of strontium feldspar (90(1) GPa by using a BM3-EoS; 84(1) GPa by using a BM2-EoS, Pandolfo et al. 2011), but meaningfully higher than those reported for alkali feldspars (all on the range 50-60 GPa, Angel 1994). In the H*P* powder diffraction study performed by Tribaudino et al. (1999) on two samples of lead feldspar with different degree of Al,Si order, the bulk modulus, calculated by using a BM2-EoS in the *P* range 0.0001 - 7.1 GPa, was 71.0(9) for the PbF1 sample ($Q_{od} = 0.68$) and 67.6 (1.2) for the PbF2 ($Q_{od} = 0.76$) sample, respectively. To compare the results obtained in the present work with those of Tribaudino et al. (1999), we have fitted our *P*-*V* data in all the *P* range 0.0001 -7.72 GPa by using a BM2-EoS: the resulting volume bulk modulus, 66(1) GPa, is quite in agreement with the results of Tribaudino et al. (1999).

Compressibilities of unit-cell axes of lead feldspar were determined by fitting a BM2-EoS to a, *b* and *c* parameters in the range 0.0001 - 4.27 GPa (grey symbols and lines in Fig. 4). The coefficients obtained are: $a_0 = 8.4008(6)$ Å, $1/3\ M_0 = 59.2(9)$ GPa; $b_0 = 13.0609(10)$ Å, $1/3\ M_0 = 99.4(1.5)$ GPa; $c_0 = 14.3347(6)$ Å, $1/3\ M_0 = 79.5(1.2)$ GPa

(with $M_i = \beta_i^{-1}$, Angel et al. 2014). The linear moduli indicate an axial compression anisotropy with $\beta a > \beta c > \beta b$. Therefore the *b* axis is less compressible than the *c* axis, that in turn is less compressible than the *a* axis. The anomalous compressional pattern at *P* higher than 4 GPa, especially evident in *a* and *c* axes, could indicate a pre-transition elastic softening. In a recent paper on compression of cordierite, Miletich et al. (2014) observed, at pressures above ~4 GPa, for *a* axis the conventional stiffening with pressure, but *b* and *c* axes reveal anomalous behavior and seem "involved in elastic softening associated with an upcoming structural instability". The elastic softening phenomenon, indicated by the negative values for $\partial(\beta^{-1})/\partial P$ coefficients, is typically associated with first-order transitions (Miletich et al. 2014).

**Phase transition**

Only two sets of unit-cell parameters were measured at pressure higher than 7.7 GPa (Table 1). At about 8 GPa the evolution of the unit-cell parameters shows a significant discontinuity (Fig. 1). The β angle suddenly decreases from 114.83 to 114.03 ° (Table 1); both *b* and *c* parameters experience a significant compression at this pressure and their relative plots show a clear step, whereas *a* parameter at about 8 GPa suddenly increases (Fig. 1). The unit-cell volume versus pressure plot (Fig. 2) does not emphasize so much the discontinuity because the volume values "merge" the two opposite trends (decrease in *b* and *c*, increase in *a*). A similar strong discontinuity in the behavior of unit-cell parameters and volumes was observed in $Ca_{0.2}Sr_{0.8}Al_2Si_2O_8$ feldspar at $P > 7.3$ GPa and in strontium feldspar at $P > 6.6$ GPa, indicating the occurrence of a phase transition strongly first-order in character (Nestola et al. 2004; Pandolfo et al. 2011). The discontinuities observed in lead feldspar in the present

work indicate the occurrence of an analogous phase transition and allow restricting its *P* range between 7.72 and 8.26 GPa. The presence of a possible phase transition for *P* > 7.1 GPa in lead feldspar had been suggested by Tribaudino et al. (1999) in a H*P* powder diffraction study. The authors observed a single monoclinic phase up to 7.1 GPa; at higher pressures, in the range 7.1 and 9.4 GPa, sudden changes in the position of the reflections occurred and some reflections appeared split, suggesting the transformation of lead feldspar to a new phase (probably feldspar-like).

In the present work the appearance of *c* and *d*- type reflections at *P* > 8 GPa, the analysis of the systematic absence and the structural refinements at *P* = 8.4 and 9.7 GPa (Table 2) indicate that the phase transition occurs from $I2/c$ to $P2_1/c$ symmetry. The $I/\sigma(I)$ ratios of the *a*, *b*, *c* and *d* superlattice reflections, collected at room pressure in lead feldspar within the DAC just before and just after the $I2/c$ - $P2_1/c$ phase transition, are listed in Table 7. The ratios are compared with those of $An_{20}SrFsp_{80}$, which is the only structure with $P2_1/c$ symmetry until now published in feldspars (Benna et al. 2007). Table 7 shows that the scheme of intensity of the different reflections in $P2_1/c$ lead feldspar is $a > d > b \geq c$, in agreement with the results observed for $An_{20}SrFsp_{80}$.

## Structural modifications

***I*2/*c* phase.** In the *P* range 0.0001 - 7.2 GPa the structural results show that the lead feldspar retains $I2/c$ symmetry with increasing pressure and the main variations are in Pb-O bond lengths and in T-O-T bond angles (Tables 5 - 6), while T-O distances and O-T-O angles does not change meaningfully, indicating that the Si,Al tetrahedra behave with pressure as a rigid body, only flexing the T-O-T angles.

The average <Pb-O> distances decrease with pressure, but some of the individual length shows an irregular evolution with a change in their compressional trend between 3 and 5 GPa (Table 5). While the Pb-$O_D$(0) distance slightly decreases and Pb-$O_D$(z) distance shows a small increase in all the *P* range, the Pb-$O_B$(z) remains quite constant until about 3 GPa, then significantly decreases (Fig. 5). The Pb-$O_C$(0) distance increases until 3 GPa and then decreases; on the contrary, the Pb-$O_B$(0) and Pb-$O_C$(z) distances decrease and then increase (Fig. 5). All the Pb-$O_A$ distances show a variation in the trend at about 6 GPa. In all the *P* range investigated, considering all individual Pb-O bond distances smaller than 2.94 Å, the coordination of the Pb site increases from sixfold at room condition (Benna et al. 1996) to a rather irregular sevenfold configuration at 7.2 GPa (Table 5).

The change in the compressional behaviour of the Pb polyhedron is obviously related to changes occurring in the T-O-T angles, because the rearrangement of the framework mainly occurs by the rotation of the essentially rigid tetrahedra, forming the characteristic crankshaft-chains running parallel to *a* axis of the feldspar structure. While the decrease of the average <T-O-T> angle with pressure is relatively small (Table 6), individual T-O-T bond angles show different variations, with some increasing and some decreasing, as typical for other feldspars studied at high pressures (Ross 2000). In the four-membered rings of tetrahedra lying on the 010 plain, forming chains parallel to *c*, the $T_1$(0)-$O_B$(0)-$T_2$(0) angle significantly decreases up to 3 GPa and then increases while $T_1$(z)-$O_B$(z)-$T_2$(z) angle slightly decreases up to 3 GPa and then slumps. The $T_1$(0)-$O_D$(0)-$T_2$(0) and $T_1$(z)-$O_D$(z)-$T_2$(z) angles remain practically constant in all the investigated *P* range.

In the other type of four-membered rings of tetrahedra, approximately normal to *a* axis, the $T_1$-$O_C$-$T_2$ angles connect the 010 tetrahedral rings along *b* direction, forming the crankshaft-chains parallel to *a*. In the low albite at H*P* (Benusa et al. 2005) these angles well describe the shear of the rings with increasing pressure. In lead feldspar the shear is not evident: the $T_1(0)$-$O_C(0)$-$T_2(0)$ angle in the *P* range 0.0001 - 7.2 GPa oscillates but on the average it decreases, while the $T_1(z)$-$O_C(z)$-$T_2(z)$ angle decreases until 3 GPa and then increases, confirming that at *P* higher than 3 GPa there is a change in the compressional trend of the framework.

In conclusion, the changes observed in the compressional behaviour of the structure between 3 and 5 GPa could explain the softening observed at $P > 4$ GPa in the volume compressibility and the BM2-EoS curve that, since this pressure, deflects from the experimental values.

***P*2$_1$/*c* phase.** The main effect of the *I*2/*c* - *P*2$_1$/*c* transition, occurring in lead feldspar at about 8 GPa, is the reduction of the symmetry with the loss of the two-fold rotation axes and of one-half of the centers of symmetry with the consequence of the doubling of the independent structural sites and the presence of pairs of atoms related by the pseudo-body centering (a + b + c) / 2 vector (Table 4).

In Fig. 6 the configurations around Pb-sites are compared in *I*2/*c* and *P*2$_1$/*c* space groups, partially projected along [001] axis. The very distorted Pb configuration at 7.2 GPa seems to be on the threshold of keeping the crystallographic equivalency of the sites. After the transition, at $P = 8.4$ GPa, the configurations of the two independent Pb(0)- and Pb(i)-sites, resulting from the doubling of the single Pb-site of the *I*2/*c* structure, show different shape, with relevant changes in the coordination

environment (Table 5). In the Pb(0)-polyhedron the larger variation concerns the two $O_C$ oxygens (mainly $O_C$(zi)) that move closer to the cation attaining the coordination sphere, whereas the $O_B$(zi) oxygen, that had significantly approached the Pb cation in the *I*2/*c* space group, slightly moves away and the two $O_D$ oxygens remain coordinated, with $O_D$(z0) that becomes very close (Fig. 6). In the Pb(i)-polyhedron the $O_C$ atoms are at distances ≥ 2.94 Å as in all other feldspars, while the bonds to the two $O_D$ atoms are broken (Pb-OD changes from 2.60 to 3.02 Å) and it is the second $O_A$(20) oxygen that becomes coordinated (Table 5). Taking into account the Pb-O distances until about 2.94 Å, the Pb(0)-site coordinates 9 oxygens, while Pb(i)-site coordinates 7 oxygens.

The differences between the unique *I*2/*c* rings of the tetrahedral framework are increased in *P*2$_1$/*c* high-pressure phase. The modifications observed are related to the significant variations of the average of the <T-$O_C$-T> angles that decreases to 118 ° at 8.4 GPa and 116 ° at 9.7 GPa (Table 6). According to Angel et al. (2005), the "hinge" of the crankshaft-chains closing up is the T-$O_C$-T angle, which undergoes the greatest decrease with increasing pressure in feldspars. In lead feldspar the $T_1$(zi)-$O_C$(zi)-$T_2$(z0) angle (Fig. 6) decreases to 110 °, a little lower than the 115 ° value, which is often considered an extreme limit for T-O-T angles in feldspars (Benusa et al. 2005). The very small value of this angle in lead feldspar at *P* = 9.7 GPa (107 °) is related to the remarkable modifications concerning the $O_C$ oxygens in the Pb(0)-polyhedron (the Pb-$O_C$(zi) distance decreases to 2.24 Å).

In *I*2/*c* configuration the four-membered rings of tetrahedra with 010 as the ring-plane are formed by the two pairs of equivalent tetrahedra; the two-fold rotation axes,

parallel to *b*, are at the centers of the rings. In $P2_1/c$ the oblique rings consist of four symmetrically non-equivalent tetrahedra, as the two-fold rotation axes are lost (Fig. 7). While in $I2/c$ the rings retain a shape almost ideally rectangular, in $P2_1/c$ the rings become irregular because of the significant variations of T-O-T angles.

The $I2/c$ - $P2_1/c$ transition induces, besides the significant distortion in the T-O-T bond angles, also a slight deformation of the internal O-T-O angles within the tetrahedra. The $T_2$(z0) tetrahedron, with the $O_A$(20)-$T_2$(z0)-$O_C$(zi) angle of 87 °, is the most deformed (Fig.6). The T-O distances instead do not shorten with the transition.

**H*P* phase transition: a comparison with alkaline-earth feldspars**

The results obtained in the present work allow comparing the pressure of the $I2/c$ - $P2_1/c$ phase transition observed in lead feldspar at $P > 8$ GPa with the pressures of the transitions occurring in the other feldspars with Al:Si ratio equal to 1:1 (i.e. alkaline-earth feldspars). As seen, the different space groups observed until now in Ca-Sr-Ba-Pb feldspars, by varying the pressure and/or the composition, are: $P\bar{1}$, $I\bar{1}$, $I2/c$ and $P2_1/c$. While at room and low pressures the $P\bar{1}$, $I\bar{1}$ and $I2/c$ phases are observed, the $P2_1/c$ phase seems to be stable only at very high pressures.

In alkaline-earth feldspars there seems to be a possible correlation between the pressure of the $I2/c$ - $P2_1/c$ transition and the dimension of the cation in the M-site. Indeed, the pressure of the transition seems to increase with the decrease of the mean ionic radius of the M cation (Ba, Sr, Ca). The $I2/c$ - $P2_1/c$ transition occurs in barium feldspar between 5.5 and 5.9 GPa (Curetti et al. 2011a), while in strontium feldspar (with $Sr^{2+}$ cation smaller than $Ba^{2+}$) it occurs at about 6.6 GPa (Pandolfo et al. 2011).

The substitution of 20% of $CaAl_2Si_2O_8$ component into the strontium feldspar structure (with a decrease in the mean ionic radius) causes an increase of the transition pressure: in the $Ca_{0.2}Sr_{0.8}Al_2Si_2O_8$ feldspar the $I2/c$ - $P2_1/c$ transition occurs at about 7.3 GPa (Nestola et al. 2004). Moreover, Pandolfo et al. (2011) hypothesized that, along the An-SrFsp join, at ~ $An_{30}SrFsp_{70}$ composition "there could be a triple point where $P2_1/c$, $I\bar{1}$ and $P\bar{1}$ phases coexist at about 7.5 GPa". Finally, Daniel et al. (1995) observed that anorthite remains $I\bar{1}$ up to 10 GPa and then transforms into a phase of higher symmetry.

The results obtained in the present work indicate that in lead feldspar the $I2/c$ - $P2_1/c$ transition occurs at about 8 GPa, a pressure higher than in strontium feldspar (6.6 GPa), although the ionic radii of Sr and Pb are similar ($^{VII}Sr^{2+}$= 1.21 Å, $^{VII}Pb^{++}$= 1.23 Å, according to Shannon 1976). Hence, lead feldspar has a higher transition pressure than could be inferred by considering only the size of the ionic radius. It is known in literature that the significant deviations of lead feldspar from trends of unit-cell parameters versus volume or ionic radius have been attributed to an effect of the lone-pair (Ribbe 1994). In lead feldspar the relatively high value of the pressure of the $I2/c$ - $P2_1/c$ transition with respect to alkaline-earth feldspars could be ascribed, besides the specific nature of $Pb^{++}$ as a lone-pair bearing cation, also to the degree of Al,Si order. We must consider that, in the lead feldspar studied at H$P$ in the present work, the Al,Si configuration is only partially ordered ($Q_{od}$ = 0.7), while the Ca-Sr-Ba feldspars studied at H$P$ are almost completely ordered, with a $Q_{od}$ = 0.9. The partial disorder occurring in lead feldspar could affect the pressure of the transition, as it was observed in anorthite, in which small amounts of disorder can affect dramatically its

phase transition behavior at H*P*. Indeed, the effect of decreasing Al,Si order on the $P\bar{1}$ - $I\bar{1}$ transition in anorthite was found to be an increase in the $P_{tr}$ and a change in the character of the transition itself (Angel 1994).

## Implications

Feldspars are major igneous and metamorphic rock-forming minerals and are among the most abundant minerals within the Earth's crust. Their H*P* and H*T* behavior is crucial for the understanding of most petrological, geochemical and thermodynamic processes. While the behavior of feldspars at elevated temperatures has been the subject of intensive investigations, yet few detailed studies have been made at elevated pressures. Pressure-induced phase transitions are very complex to model because they are "non-quenchable" and therefore require "in situ" studies at H*P* for their characterization. Although feldspars are stable in an extremely limited pressure range under geological conditions, compressional studies and investigations on phase transitions induced by pressure can provide more accurate EoS data on thermodynamic properties useful for petrological applications (Angel 1994).

In the present work we have measured the compressibility of lead feldspar by single-crystal in situ XRD techniques and we have found a new $P2_1/c$ phase at $P > 8$ GPa. The experimental findings of this study improve the knowledge on the elastic behavior at H*P* of feldspars with Al:Si ratio equal to 1:1 and provide new compressibility data for their thermodynamic characterization, as well as a basis for further H*P* structural studies. As the state of Al,Si order can affect the elastic properties and EoS (e.g. the bulk modulus increases from sanidine to microcline), we suggest that the different degree of Al,Si order may also affect the pressure of the $I2/c$ – $P2_1/c$

displacive transition that occurs at very high pressure in Ca-Sr-Pb-Ba- feldspars. Further investigations at H*P* on lead feldspar with different degrees of Al,Si order are needed, with the aim to study the interactions between slow order-disorder processes and fast displacive phase transitions.

To extend our investigation's implications to the geological context, lead feldspar represents a useful model for characterizing the thermodynamic behavior of anorthite and anorthite-bearing feldspars. Indeed, it is well known that anorthite retains an ordered Al,Si configuration up to a temperature close to the melting point, and only limited changes in Al,Si ordering can be achieved by extreme heating (Benna et al. 1985; Carpenter 1992). On the contrary, in lead feldspar the Al,Si ordering kinetics are significantly faster and a significant degree of Al,Si disorder (that can not be reached in anorthite) can be easily achieved at low temperatures by varying the annealing conditions (Tribaudino et al. 1998) .

## Acknowledgments

The authors thank Fabrizio Nestola, Ross J. Angel and Matteo Alvaro for helpful suggestions. Ross J. Angel is sincerely thanked for installing SINGLE software at Department of Earth Sciences, University of Torino. Reviews from two anonymous referees greatly improved the manuscript; we are grateful to them for critical reading and useful suggestions. We thank associate editor Diego Gatta. The "Scansetti" and "CrisDi" Interdepartmental Centres of University of Torino are thanked. Financial support has been provided by MIUR (Roma).

## References cited

Allan, D.R., and Angel, R.J. (1997) A high-pressure structural study of microcline ($KAlSi_3O_8$) to 7 GPa. European Journal of Mineralogy, 9, 263-275.

Angel, R.J. (1992) Order-disorder and the high-pressure $P\bar{1}$ - $I\bar{1}$ transition in anorthite. American Mineralogist, 77, 923-929.

——— (1994) Feldspars at high pressure. In I. Parsons, Ed., Feldspars and their Reactions, p. 271-312. Kluwer, Dordrecht, The Netherlands.

——— (2000) Equations of state. In R.M. Hazen and R.T. Downs, Eds., High-Temperature and High-Pressure Crystal Chemistry, 41, p. 35-59. Reviews in Mineralogy and Geochemistry, Mineralogical Society of America and Geochemical Society, Chantilly, Virginia.

——— (2004) Equations of state of plagioclase feldspars. Contributions to Mineralogy and Petrology, 146, 506-512.

Angel, R.J., and Finger, L.W. (2011) SINGLE: a program to control single-crystal diffractometers. Journal of Applied Crystallography, 44, 247-251.

Angel, R.J., and Gonzalez-Platas J. (2013) ABSORB-7 and ABSORB-GUI for single-crystal absorption corrections. Journal of Applied Crystallography, 46, 252-254.

Angel, R.J., Hazen, R.M., McCormick, T.C., Prewitt, C.T., and Smyth, J.R. (1988) Comparative compressibility of end-member feldspars. Physics and Chemistry of Minerals, 15, 313-318.

Angel, R.J., Carpenter, M.A., and Finger, L.W. (1990) Structural variation associated with compositional variation and order-disorder behavior in anorthite-rich feldspars. American Mineralogist, 75, 150-162.

Angel, R.J., Downs, R.T., and Finger, L.W. (2000) High-temperature - high-pressure diffractometry. In R.M. Hazen and R.T. Downs, Eds., High-Temperature and High-Pressure Crystal Chemistry, 41, p. 559-596. Reviews in Mineralogy and Geochemistry, Mineralogical Society of America and Geochemical Society, Chantilly, Virginia.

Angel, R.J., Ross, N.L., and Zhao, J. (2005) The compression of framework minerals: beyond rigid polyhedra. European Journal of Mineralogy, 17, 193-199.

Angel, R.J., Gonzalez-Platas, J., and Alvaro, M. (2014) EosFit7c and a Fortran module (library) for equation of state calculations. Zeitschrift für Kristallographie, 229, 405-419.

Bambauer, H.U., and Nager, H.E. (1981) Gitterkonstanten und displazive Transformationen synthetischer Erdalkalifeldspäte. I. System $Ca[Al_2Si_2O_8]$-$Sr[Al_2Si_2O_8]$-$Ba[Al_2Si_2O_8]$. Neues Jahrbuch für Mineralogie Abhandlungen, 141, 225-239 (in German).

Benna, P., and Bruno, E. (2003) Single-crystal in situ high-temperature structural investigation of the $I\bar{1}$ - I2/c phase transition in $Ca_{0.2}Sr_{0.8}Al_2Si_2O_8$ feldspar. American Mineralogist, 88, 1532-1541.

Benna, P., Zanini, G., and Bruno, E. (1985) Cell parameters of thermally treated anorthite. Al, Si configurations in the average structures of the high temperature calcic plagioclases. Contributions to Mineralogy and Petrology, 90, 381-385.

Benna, P., Tribaudino, M., and Bruno, E. (1996) The structure of ordered and disordered lead feldspar ($PbAl_2Si_2O_8$). American Mineralogist, 81, 1337-1343.

——— (2000) $I\bar{1}$ - I2/c ferroelastic phase transition in the $Ca_{0.2}Pb_{0.8}Al_2Si_2O_8$ feldspar as a function of temperature. Mineralogical Magazine, 64, 285-290.

Benna, P., Nestola, F., Boffa Ballaran, T., Balić-Žunić, T., Fahl Lundegaard, L., and Bruno, E. (2007) The high-pressure structural configurations of $Ca_{0.2}Sr_{0.8}Al_2Si_2O_8$ feldspar: the $I\bar{1}$ - I2/c and I2/c - $P2_1/c$ phase transitions. American Mineralogist, 92, 1190-1199.

Benusa, M.D., Angel, R.J., and Ross, N.L. (2005) Compression of albite $NaAlSi_3O_8$. American Mineralogist, 90, 1115-1120.

Bruno, E., and Facchinelli, A. (1972) Al, Si configurations in lead feldspar. Zeitschrift für Kristallographie, 136, 296-304.

Bruno, E., and Gazzoni, G. (1968) Feldspati sintetici della serie $CaAl_2Si_2O_8$-$SrAl_2Si_2O_8$. Atti dell'Accademia delle Scienze di Torino, 102, 881-893 (in Italian).

Carpenter, M.A. (1992) Equilibrium thermodynamics of Al/Si ordering in anorthite. Physics and Chemistry of Minerals, 19, 1-24.

Chiari, G., Calleri, M., Bruno, E., and Ribbe, P.H. (1975) The structure of partially disordered synthetic strontium feldspar. American Mineralogist, 60, 111-119.

Curetti, N., Benna, P., Nestola, F., and Bruno, E. (2011a) High-pressure structural configurations of celsian. Geoitalia 2011, VIII Forum Italiano di Scienze della Terra (FIST), Epitome, 213, 4, Torino, ISSN 1972-1552.

Curetti, N., Sochalski-Kolbus, L., Angel, R.J., Benna, P., Nestola, F., and Bruno, E. (2011b) High-pressure structural evolution and equation of state of analbite. American Mineralogist, 96, 383-392.

Daniel, I., Gillet, P., and Ghose, S. (1995) A new high pressure phase transition in anorthite ($CaAl_2Si_2O_8$) revealed by Raman spectroscopy. American Mineralogist, 80, 645-648.

Downs, R.T., Hazen, R.M., and Finger, L.W. (1994) The high pressure crystal chemistry of low albite and the origin of the pressure dependency of Al-Si ordering. American Mineralogist, 79, 1042-1052.

Hackwell, T.P., and Angel, R.J. (1992) The comparative compressibility of reedmergnerite, danburite and their aluminum analogues. European Journal of Mineralogy 4,1221-1227.

King, H.E., and Finger, L.W. (1979) Diffracted beam crystal centering and its application to high pressure crystallography. Journal of Applied Crystallography, 12, 374-378.

Mao, H.K., Xu, J., and Bell, P.M. (1986) Calibration of the ruby pressure gauge to 800 kbar under quasi-hydrostatic conditions. Journal of Geophysical Research, 91, 4673-4676.

McGuinn, M.D., and Redfern, S.A.T. (1994) Ferroelastic phase transition along the join $CaAl_2Si_2O_8$-$SrAl_2Si_2O_8$. American Mineralogist, 79, 24-30.

——— (1997) High-temperature ferroelastic strain below the I2/c - $I\bar{1}$ transition in $Ca_{1-x}Sr_xAl_2Si_2O_8$ feldspars. European Journal of Mineralogy, 9, 1159-1172.

Megaw, H.D., Kempster, C.J.E., and Radoslovich, E.W. (1962) The structure of anorthite $CaAl_2Si_2O_8$. II. Description and discussion. Acta Crystallographica, 15, 1017-1035.

Miletich, R., Alla, D.R ., and Kuhs, W. F. (2000) High pressure single-crystal technique. In R.M. Hazen and R.T. Downs, Eds., High-Temperature and High Pressure Crystal Chemistry, 41, p. 445-520. Review in Mineralogy and Geochemistry, Mineralogical Society and Geochemical Society, Chantilly, Virginia.

Miletich, R., Gatta, G.D., Willi, T., Mirwald, P.W., Lotti, P., Merlini, M., Rotiroti**,** N., and Loerting, T. (2014) Cordierite under hydrostatic compression: Anomalous elastic behavior as a precursor for a pressure-induced phase transition. American Mineralogist, 99, 479-493.

Mrosko, M., Koch-Muller, M., and Schade, U. (2011) In-situ mid/far micro-FTIR spectroscopy to trace pressure-induced phase transitions in strontium feldspar and wadsleyite. American Mineralogist, 96, 1748-1759.

Nager, H.E., Hoffmann, W., and Nissen, H.U. (1969) Die Mischreihe (Ca,Sr)[$Al_2Si_2O_8$]. Naturwissenschaften 56, 136 (in German).

Nestola, F., Boffa Ballaran, T., Benna, P., Tribaudino, M., and Bruno, E. (2004) High-pressure phase transitions in $Ca_{0.2}Sr_{0.8}Al_2Si_2O_8$ feldspar. American Mineralogist, 89, 1474-1479.

Nestola, F., Curetti, N., Benna, P., Ivaldi, G., Angel, R.J., and Bruno, E. (2008) Compressibility and high-pressure behavior of $Ab_{63}Or_{27}An_{10}$ anorthoclase. Canadian Mineralogist, 46, 1443-1454.

Newman, R.E., and Megaw, H.D. (1960) The crystal structure of celsian (barium feldspar). Acta Crystallographica, 13, 303-312.

Pandolfo, F., Ballaran, T.B., Nestola, F., Muller, M.K., Mrosko, M., and Bruno, E. (2011) High-pressure I2/c-$P2_1/c$ phase transformation in $SrAl_2Si_2O_8$ feldspar. American Mineralogist, 96, 1182-1185.

Phillips, B.L., McGuinn, M.D., and Redfern S.A.T. (1997) Si-Al order and the $I\bar{1}$ - I2/c structural phase transition in synthetic $CaAl_2Si_2O_8$ - $SrAl_2Si_2O_8$ feldspar: A $^{29}Si$ MAS-NMR spectroscopy study. American Mineralogist, 82, 1-7.

Ribbe, P.H. (1994) The crystal structures of the aluminum-silicate feldspars. In I. Parsons, Ed., Feldspars and Their Reactions, p. 1-49. Kluwer Academic Publishers, Dordrecht.

Ross, N.L. (2000) Framework structures. In R.M. Hazen and R.T. Downs, Eds., High-Temperature and High-Pressure Crystal Chemistry, p. 257-287. Reviews in Mineralogy

and Geochemistry, Mineralogical Society of America and Geochemical Society, Chantilly, Virginia.

Shannon, R.D. (1976) Revised effective ionic radii and systematic studies of interatomic distances in halides and chalcogenides. Acta Crystallographica, 32, 751-767.

Sheldrick, G.M. (2008) A short history of SHELX. Acta Crystallographica, A64, 112-122.

Sochalski-Kolbus, L.M., Angel, R.J., and Nestola, F. (2010) The effect of Al/Si disorder on the bulk moduli of plagioclase feldspars. Mineralogical Magazine, 74, 943-950.

Tribaudino, M., Benna, P., and Bruno, E. (1993) $I\bar{1}$-I2/c phase transition in alkaline-earth feldspars along the $CaAl_2Si_2O_8$-$SrAl_2Si_2O_8$ join: Thermodynamic behaviour. Physics and Chemistry of Minerals, 20, 221-227.

——— (1998) Structural variations induced by thermal treatment in lead feldspar ($PbAl_2Si_2O_8$). American Mineralogist, 83, 159-166.

Tribaudino, M., Benna, P., Bruno, E., and Hanfland, M. (1999) High pressure behaviour of lead feldspar ($PbAl_2Si_2O_8$). Physics and Chemistry of Minerals, 26, 367-37.

Tribaudino, M., Benna, P., and Bruno, E. (2000) TEM observations on the $P\bar{1}$ - $I\bar{1}$ phase transition in feldspars along the join $CaAl_2Si_2O_8$-$SrAl_2Si_2O_8$. American Mineralogist, 85, 963-970.

Tribaudino, M., Benna, P., Nestola, F., Meneghini, C., and Bruno, E. (2005) Thermodynamic behaviour of the high-temperature $P\bar{1}$ - $I\bar{1}$ phase transition along the $CaAl_2Si_2O_8$-$SrAl_2Si_2O_8$ join. Physics and Chemistry of Minerals, 32, 314-321.

Tribaudino, M., Zhang, M., and Salje, E.K.H. (2009) Cation ordering and phase transitions in feldspars along the join $CaAl_2Si_2O_8$-$SrAl_2Si_2O_8$: a TEM, IR and XRD investigation. Mineralogical Magazine, 73, 119-130.

## Figure Captions

**Figure 1.** The variations of the *a*, *b*, *c* and β unit-cell parameters of lead feldspar with pressure. Grey circle: $I2/c$ phase. Black circle: $P2_1/c$ high-pressure phase. Experimental uncertainties are smaller than symbols.

**Figure 2.** The variation of the unit-cell volume of lead feldspar with pressure. Symbols as in Fig. 1. The line shows the second-order Birch-Murnaghan equation of state (BM2-EoS) in the *P* range 0.0001 - 4.27 GPa. Experimental uncertainties are smaller than symbols.

**Figure 3.** Evolution of the normalized pressure $F_E$ versus Eulerian finite strain $f_E$ in lead feldspar. $F_E = P/3 \times f_E \times (1 + 2 f_E)^{5/2}$ and $f_E = [(V_O/V)^{2/3} - 1] / 2$ (Angel 2000). The horizontal line of constant $F_E$ indicates that the *P*-*V* data (grey circles, *P* range 0.0001 - 4.27 GPa) could be fitted by a second-order truncation of the BM-EoS. Open circles: *P*-*V* data in the range 4.79 - 7.72 GPa.

**Figure 4.** The variations of the *a*, *b*, *c* lattice edges of lead feldspar as a function of pressure, normalized to their room pressure values. Diamonds: $a/a_0$; squares: $b/b_0$; circles: $c/c_0$. Lines correspond to linear fits in the *P* range 0.0001 - 4.27 GPa (grey symbols) with linear moduli $M_i$ = 177.5(2.7), 298.1(4.6), 238.5(3.6) GPa, respectively (with i = *a*, *b*, *c* and $M_i = \beta_i^{-1}$, Angel et al. 2014). Open circles: normalized parameters the range 4.79 - 7.72 GPa. Experimental uncertainties are smaller than symbols.

**Figure 5.** The variations of the Pb-$O_B$ and Pb-$O_C$ distances with pressure in the *P* range 0.0001 - 7.2 GPa. Circles: $O_B$; squares: $O_C$ atoms. The lines are drawn as guides to the eye.

**Figure 6.** Partial projections along [001] of the M-site configurations at different pressures ("dog face projection", thickness ~ 3.5 Å). Atoms in the shadow: $I2/c$ space group at $P$ = 7.2 GPa. Atoms in close-up: $P2_1/c$ space group at $P$ = 8.4 GPa. Grey label refers to $I2/c$, black label to $P2_1/c$ space group. In $P2_1/c$ symmetry the single Pb-site is doubled in two independent Pb(0)- and Pb(i)-sites. In Pb(0) the $O_C$(zi) and the two $O_D$ oxygens are coordinated; the arrows indicate the smallest $T_2$(z0)-$O_C$(zi)-$T_1$(zi) angle (110 °) and the most deformed $T_2$(z0) tetrahedron, with the $O_A$(20)-$T_2$(z0)-$O_C$(zi) angle of 87 °. In Pb(i) the two $O_D$ oxygens , that were coordinated in $I2/c$, move away (the change in $O_D$(0i) is indicated).

**Figure 7.** The four-membered rings of tetrahedra with 010 as the ring-plane, forming chains parallel to $c$. Projection on the 010 plane (thickness ~ 5 Å). $O_C$ oxygens are not shown. Atoms in the shadow: $P$ = 7.2 GPa, $I2/c$ space group; the two-fold rotation axes, parallel to $b$, are at the centers of the rings formed by the two pairs of equivalent tetrahedra. Atoms in close-up: $P$ = 8.4 GPa, $P2_1/c$ space group; the rings consist of four symmetrically non-equivalent tetrahedra, as the two-fold rotation axes are lost; the structure is more free and the rings become more irregular. The largest angles are $T_1$(0i)-$O_B$(0i)-$T_2$(0i) (156 °) and $T_1$(zi)-$O_D$(zi)-$T_2$(z0) (162 °).

Table 1. Unit-cell parameters of lead feldspar as a function of pressure ($\sigma P$ = 0.1 GPa) (esd in brackets)

| *P* (GPa) | *a* (Å) | *b* (Å) | *c* (Å) | β (°) | *V* (Å³) |
|---|---|---|---|---|---|
| 0.0001 | 8.4004(6) | 13.0604(13) | 14.3339(6) | 115.268(3) | 1422.1(2) |
| 0.0001 [a] | 8.4002(9) | 13.0611(18) | 14.3354(8) | 115.278(4) | 1422.2(2) |
| 0.24 | 8.3950(5) | 13.0544(13) | 14.3270(5) | 115.274(2) | 1419.8(2) |
| 0.28 | 8.3923(9) | 13.046(2) | 14.3221(9) | 115.286(5) | 1417.8(3) |
| 0.50 | 8.3811(6) | 13.0413(14) | 14.3094(5) | 115.295(3) | 1414.1(2) |
| 1.02 | 8.3604(9) | 13.009(3) | 14.2841(10) | 115.302(5) | 1404.5(3) |
| 1.16 | 8.3502(4) | 13.0107(10) | 14.2698(4) | 115.310(2) | 1401.5(1) |
| 1.79 [a] | 8.3267(8) | 12.9891(19) | 14.2384(9) | 115.315(5) | 1392.1(2) |
| 1.98 | 8.3197(6) | 12.9775(16) | 14.2278(6) | 115.305(3) | 1388.8(2) |
| 2.09 | 8.3177(5) | 12.9759(12) | 14.2269(5) | 115.309(2) | 1388.1(2) |
| 2.27 [a] | 8.3042(9) | 12.970(2) | 14.2119(11) | 115.291(6) | 1383.9(3) |
| 3.00 | 8.2763(21) | 12.940(4) | 14.174(3) | 115.291(13) | 1372.4(6) |
| 3.06 | 8.2698(6) | 12.9334(13) | 14.1664(5) | 115.282(3) | 1370.1(2) |
| 3.31 [a] | 8.2585(6) | 12.9266(15) | 14.1490(8) | 115.273(4) | 1365.9(2) |
| 3.83 [a] | 8.2338(12) | 12.903(3) | 14.1172(13) | 115.221(6) | 1356.9(3) |
| 4.27 | 8.2195(7) | 12.8878(16) | 14.0947(6) | 115.195(3) | 1351.0(2) |
| 4.79 | 8.1905(17) | 12.864(3) | 14.0553(15) | 115.168(8) | 1340.4(4) |
| 5.13 | 8.1720(9) | 12.854(2) | 14.0228(8) | 115.098(5) | 1333.9(3) |
| 5.62 | 8.1448(10) | 12.828(3) | 13.9858(9) | 115.043(5) | 1323.8(4) |
| 5.98 | 8.1201(9) | 12.811(2) | 13.9460(7) | 114.994(4) | 1314.9(3) |
| 6.66 | 8.0875(10) | 12.792(2) | 13.8946(8) | 114.933(5) | 1303.5(3) |
| 7.01 | 8.0722(10) | 12.781(2) | 13.8728(8) | 114.907(5) | 1298.1(3) |
| 7.32 | 8.0562(11) | 12.767(3) | 13.8448(9) | 114.870(5) | 1292.0(3) |
| 7.53 | 8.0501(14) | 12.751(3) | 13.8227(12) | 114.842(6) | 1287.6(4) |
| 7.72 | 8.0391(15) | 12.746(4) | 13.8119(13) | 114.830(7) | 1284.5(5) |
| 8.26 [b] | 8.056(2) | 12.567(3) | 13.719(2) | 114.028(11) | 1268.6(5) |
| 8.35 [b] | 8.050(3) | 12.554(5) | 13.702(3) | 113.980(14) | 1265.1(6) |

*Notes:* [a] Measured in decreasing pressure. [b] $P2_1/c$ space group.

Table 2. Single-crystal data at different pressures

| *P* (GPa) | 0.0001 [a] | 2.4 | 3.1 | 5.4 | 6.0 | 7.2 | 8.4 | 9.7 |
|---|---|---|---|---|---|---|---|---|
| Space group | *I*2/*c* | *I*2/*c* | *I*2/*c* | *I*2/*c* | *I*2/*c* | *I*2/*c* | $P2_1/c$ | $P2_1/c$ |
| *a* (Å) | 8.3941(4) | 8.3214(8) | 8.2783(11) | 8.160(3) | 8.1063(13) | 8.086(4) | 8.057(1) | 8.0401(15) |
| *b* (Å) | 13.022(11) | 12.979(14) | 12.94(2) | 12.84(3) | 12.86(2) | 12.73(4) | 12.515(14) | 12.41(2) |
| *c* (Å) | 14.3153(7) | 14.2352(14) | 14.1774(18) | 14.024(3) | 13.920(3) | 13.858(6) | 13.7079(16) | 13.593(2) |
| β (°) | 115.253(6) | 115.336(12) | 115.269(16) | 115.08(3) | 114.94(2) | 114.90(5) | 114.116(14) | 113.997(19) |
| $V$ (Å$^3$) | 1415(1) | 1390(2) | 1373(2) | 1331(3) | 1316(2) | 1294(4) | 1262(1) | 1239(2) |
| Unique refl. | 634 | 527 | 441 | 456 | 470 | 434 | 1120 | 842 |
| Refl. $F_0 \geq 4\sigma(F_0)$ | 537 | 432 | 376 | 354 | 357 | 416 | 743 | 575 |
| $R$ $F_0 \geq 1\sigma(F_0)$ | 7.01 | 7.00 | 8.34 | 7.62 | 10.48 | 14.96 | 17.40 | 17.27 |
| $R$ $F_0 \geq 4\sigma(F_0)$ | 5.67 | 4.80 | 6.55 | 5.27 | 7.18 | 14.48 | 10.38 | 11.23 |
| Weight | 0.12 | 0.11 | 0.15 | 0.14 | 0.17 | 0.32 | 0.25 | 0.27 |
| Goodness of fit | 1.29 | 1.28 | 1.27 | 1.04 | 1.16 | 1.16 | 1.14 | 1.20 |

*Note*: [a] within the DAC; $w = 1 / [\sigma^2(F_0^2) + (a \cdot P)^2]$, where $P = (F_0^2 + 2F_c^2) / 3$.

Table 3. Atomic fractional coordinates and displacement parameters (Å$^2$) for *I*2/*c* lead feldspar at different pressures

| *P* (GPa) | Site | *x* | *y* | *z* | $U_{iso}/U_{eq}$ [a] | Site | *x* | *y* | *z* | $U_{iso}$ |
|---|---|---|---|---|---|---|---|---|---|---|
| 0.0001 | Pb | 0.2726(1) | -0.0041(2) | 0.0718(1) | 0.0523(17) | | | | | |
| 2.4 | | 0.2707(1) | -0.0005(6) | 0.0699(1) | 0.0519(15) | | | | | |
| 3.1 | | 0.2702(2) | -0.0032(9) | 0.0696(1) | 0.054(3) | | | | | |
| 5.4 | | 0.2690(2) | -0.0045(6) | 0.0700(1) | 0.0463(16) | | | | | |
| 6.0 | | 0.2684(2) | -0.0049(9) | 0.0701(1) | 0.067(3) | | | | | |
| 7.2 | | 0.2675(4) | -0.0039(8) | 0.0704(2) | 0.062(5) | | | | | |
| 0.0001 | T1(0) | 0.0048(5) | 0.1862(13) | 0.1097(3) | 0.0124(9) | T1(z) | 0.0046(5) | 0.1732(15) | 0.6151(3) | 0.0091(10) |
| 2.4 | | -0.0006(11) | 0.165(2) | 0.1077(6) | 0.019(3) | | 0.0028(9) | 0.194(2) | 0.6156(5) | 0.006(2) |
| 3.1 | | -0.0080(17) | 0.160(3) | 0.1090(9) | 0.022(4) | | 0.0058(15) | 0.198(3) | 0.6145(8) | 0.006(3) |
| 5.4 | | 0.0102(11) | 0.1751(19) | 0.1165(6) | 0.017(2) | | -0.0275(16) | 0.188(2) | 0.6051(7) | 0.026(3) |
| 6.0 | | 0.0114(13) | 0.178(2) | 0.1162(8) | 0.023(2) | | -0.0297(15) | 0.184(2) | 0.6061(8) | 0.021(2) |
| 7.2 | | 0.0009(14) | 0.174(3) | 0.1080(8) | 0.004(3) | | -0.031(2) | 0.186(3) | 0.6166(13) | 0.026(4) |
| 0.0001 | T2(0) | 0.6957(5) | 0.1170(12) | 0.1729(3) | 0.0089(8) | T2(z) | 0.6867(5) | 0.1159(12) | 0.6725(3) | 0.0136(8) |
| 2.4 | | 0.6893(11) | 0.127(2) | 0.1725(7) | 0.012(3) | | 0.6863(12) | 0.1039(19) | 0.6719(7) | 0.017(3) |
| 3.1 | | 0.6855(19) | 0.134(3) | 0.1723(10) | 0.021(4) | | 0.6875(15) | 0.105(3) | 0.6726(8) | 0.014(3) |
| 5.4 | | 0.6687(13) | 0.113(2) | 0.1704(7) | 0.022(3) | | 0.6967(14) | 0.124(2) | 0.6747(7) | 0.022(2) |
| 6.0 | | 0.6702(17) | 0.123(3) | 0.1698(11) | 0.033(4) | | 0.6941(15) | 0.114(3) | 0.6756(9) | 0.028(3) |
| 7.2 | | 0.675(2) | 0.118(4) | 0.1773(14) | 0.035(5) | | 0.6910(17) | 0.113(3) | 0.6719(10) | 0.019(3) |

Continues

| | | | | | | | | | | |
|---|---|---|---|---|---|---|---|---|---|---|
| 0.0001 | OA(1) | -0.0032(12) | 0.134(3) | -0.0015(7) | 0.0157(19) | OA(2) | 0.5984(13) | -0.005(3) | 0.1460(7) | 0.020(2) |
| 2.4 | | -0.015(3) | 0.139(3) | -0.0070(14) | 0.015(3) | | 0.5945(16) | 0.008(3) | 0.1472(9) | 0.018(3) |
| 3.1 | | -0.007(6) | 0.140(5) | -0.003(2) | 0.023(5) | | 0.595(3) | 0.011(4) | 0.1481(16) | 0.028(5) |
| 5.4 | | -0.021(2) | 0.140(3) | -0.0059(13) | 0.014(4) | | 0.590(3) | -0.013(3) | 0.1554(19) | 0.055(7) |
| 6.0 | | -0.022(3) | 0.140(4) | -0.0035(19) | 0.027(5) | | 0.596(5) | -0.002(4) | 0.158(3) | 0.072(10) |
| 7.2 | | 0.014(4) | 0.146(6) | -0.002(2) | 0.025(9) | | 0.571(8) | -0.004(4) | 0.145(5) | 0.08(2) |
| 0.0001 | OB(0) | 0.8258(13) | 0.129(3) | 0.1095(7) | 0.022(2) | OB(z) | 0.8108(14) | 0.134(3) | 0.6130(8) | 0.027(3) |
| 2.4 | | 0.823(3) | 0.112(5) | 0.111(2) | 0.039(9) | | 0.806(2) | 0.144(4) | 0.6080(13) | 0.015(5) |
| 3.1 | | 0.811(3) | 0.106(5) | 0.1071(17) | 0.007(5) | | 0.807(6) | 0.145(8) | 0.607(3) | 0.055(15) |
| 5.4 | | 0.794(3) | 0.161(5) | 0.1031(18) | 0.033(6) | | 0.810(3) | 0.102(4) | 0.6019(18) | 0.033(6) |
| 6.0 | | 0.796(3) | 0.172(7) | 0.104(2) | 0.048(9) | | 0.803(3) | 0.098(4) | 0.600(2) | 0.035(7) |
| 7.2 | | 0.807(7) | 0.152(14) | 0.112(5) | 0.09(2) | | 0.796(4) | 0.097(5) | 0.596(2) | 0.015(8) |
| 0.0001 | OC(0) | 0.0240(18) | 0.310(4) | 0.1283(10) | 0.036(4) | OC(z) | 0.0150(12) | 0.301(3) | 0.6278(7) | 0.011(2) |
| 2.4 | | 0.004(4) | 0.293(3) | 0.128(2) | 0.053(10) | | 0.014(2) | 0.321(3) | 0.6281(13) | 0.012(4) |
| 3.1 | | 0.008(6) | 0.284(4) | 0.128(4) | 0.073(19) | | 0.004(3) | 0.327(3) | 0.629(2) | 0.016(6) |
| 5.4 | | -0.013(3) | 0.302(3) | 0.1156(19) | 0.033(6) | | 0.006(3) | 0.317(3) | 0.641(2) | 0.039(7) |
| 6.0 | | -0.017(5) | 0.305(4) | 0.115(3) | 0.060(12) | | 0.008(4) | 0.316(3) | 0.636(2) | 0.042(8) |
| 7.2 | | -0.012(3) | 0.303(4) | 0.1190(19) | 0.000(6) | | 0.013(6) | 0.315(4) | 0.649(4) | 0.056(15) |
| 0.0001 | OD(0) | 0.1874(13) | 0.128(3) | 0.1973(7) | 0.021(2) | OD(z) | 0.1952(13) | 0.121(3) | 0.7003(7) | 0.020(2) |
| 2.4 | | 0.193(2) | 0.134(4) | 0.1934(13) | 0.016(5) | | 0.185(2) | 0.127(4) | 0.7064(14) | 0.020(5) |
| 3.1 | | 0.176(3) | 0.110(5) | 0.2034(15) | 0.011(6) | | 0.203(4) | 0.138(6) | 0.6985(19) | 0.023(7) |
| 5.4 | | 0.175(5) | 0.109(6) | 0.200(3) | 0.095(19) | | 0.185(2) | 0.134(4) | 0.7011(11) | 0.012(4) |
| 6.0 | | 0.168(4) | 0.107(5) | 0.204(2) | 0.051(11) | | 0.190(3) | 0.143(6) | 0.6983(18) | 0.030(7) |
| 7.2 | | 0.164(5) | 0.102(6) | 0.196(2) | 0.038(11) | | 0.188(7) | 0.145(11) | 0.703(4) | 0.08(2) |

*Note*: All atoms except for Pb were refined with isotropic displacement parameters. [a] $U_{eq}$ defined as one third of the trace of the orthogonalized $U_{ij}$ tensor.

Table 4. Atomic fractional coordinates and isotropic displacement coefficients (Å$^2$) for $P2_1/c$ lead feldspar at different pressures

| | $P$ = 8.4 GPa | | | | $P$ = 9.7 GPa | | | |
|---|---|---|---|---|---|---|---|---|
| Site | $x$ | $y$ | $z$ | $U_{iso}/U_{eq}$[a] | $x$ | $y$ | $z$ | $U_{iso}/U_{eq}$[a] |
| Pb(0) | 0.2878(2) | -0.0035(7) | 0.0695(1) | 0.050(3) | 0.2882(3) | -0.0091(11) | 0.0691(2) | 0.063(5) |
| Pb(i) | 0.7604(2) | 0.5024(6) | 0.5689(1) | 0.051(3) | 0.7610(3) | 0.4999(10) | 0.5683(2) | 0.075(5) |
| T1(00) | 0.9968(13) | 0.173(2) | 0.1187(7) | 0.011(2) | 0.012(3) | 0.178(5) | 0.1155(19) | 0.041(7) |
| T1(0i) | 0.4838(17) | 0.683(3) | 0.6108(10) | 0.026(3) | 0.480(3) | 0.678(5) | 0.6088(17) | 0.029(6) |
| T1(z0) | -0.001(3) | 0.173(4) | 0.6114(15) | 0.053(6) | -0.013(3) | 0.166(5) | 0.6214(16) | 0.023(5) |
| T1(zi) | 0.4779(16) | 0.711(3) | 0.0962(10) | 0.021(3) | 0.474(3) | 0.709(6) | 0.0941(19) | 0.034(7) |
| T2(00) | 0.6916(12) | 0.121(2) | 0.1838(7) | 0.0024(19) | 0.696(2) | 0.129(3) | 0.1886(11) | 0.004(3) |
| T2(0i) | 0.184(3) | 0.618(4) | 0.6743(14) | 0.049(5) | 0.165(5) | 0.614(6) | 0.674(3) | 0.060(10) |
| T2(z0) | 0.695(3) | 0.120(5) | 0.6736(17) | 0.076(7) | 0.690(4) | 0.109(6) | 0.671(2) | 0.058(9) |
| T2(zi) | 0.1702(14) | 0.627(3) | 0.1711(8) | 0.015(2) | 0.177(2) | 0.631(4) | 0.1676(13) | 0.013(4) |
| OA(10) | -0.016(4) | 0.135(6) | -0.0055(18) | 0.021(7) | -0.020(6) | 0.125(7) | -0.013(3) | 0.025(12) |
| OA(1i) | 0.495(4) | 0.645(8) | 0.499(2) | 0.041(10) | 0.488(5) | 0.639(9) | 0.488(3) | 0.016(10) |
| OA(20) | 0.622(5) | 0.008(5) | 0.199(3) | 0.052(9) | 0.609(7) | -0.003(6) | 0.198(4) | 0.054(15) |
| OA(2i) | 0.081(4) | 0.505(5) | 0.632(2) | 0.035(7) | 0.075(6) | 0.513(6) | 0.625(4) | 0.050(14) |

continues

| | | | | | | | | |
|---|---|---|---|---|---|---|---|---|
| OB(00) | 0.777(8) | 0.144(14) | 0.082(5) | 0.13(3) | 0.796(8) | 0.153(16) | 0.095(5) | 0.07(2) |
| OB(0i) | 0.315(4) | 0.642(7) | 0.619(2) | 0.027(7) | 0.291(8) | 0.693(11) | 0.622(6) | 0.07(2) |
| OB(z0) | 0.812(3) | 0.107(5) | 0.6094(17) | 0.012(5) | 0.806(9) | 0.078(10) | 0.609(6) | 0.09(3) |
| OB(zi) | 0.271(3) | 0.640(6) | 0.084(2) | 0.023(7) | 0.292(6) | 0.636(9) | 0.096(4) | 0.032(12) |
| OC(00) | 0.992(4) | 0.296(5) | 0.156(2) | 0.032(8) | 0.990(5) | 0.296(6) | 0.161(3) | 0.015(9) |
| OC(0i) | 0.494(7) | 0.806(6) | 0.622(4) | 0.09(2) | 0.496(5) | 0.809(6) | 0.629(3) | 0.023(11) |
| OC(z0) | 0.985(3) | 0.308(5) | 0.6279(19) | 0.013(6) | -0.013(5) | 0.300(6) | 0.624(3) | 0.010(8) |
| OC(zi) | 0.497(4) | 0.848(5) | 0.113(2) | 0.035(9) | 0.477(6) | 0.851(7) | 0.093(4) | 0.032(13) |
| OD(00) | 0.187(4) | 0.111(6) | 0.2036(19) | 0.024(7) | 0.186(5) | 0.100(8) | 0.200(3) | 0.024(11) |
| OD(0i) | 0.679(5) | 0.680(9) | 0.692(3) | 0.068(14) | 0.663(7) | 0.708(9) | 0.701(4) | 0.052(19) |
| OD(z0) | 0.208(6) | 0.114(9) | 0.701(3) | 0.067(14) | 0.215(10) | 0.185(14) | 0.709(5) | 0.13(5) |
| OD(zi) | 0.663(4) | 0.657(7) | 0.203(2) | 0.040(9) | 0.656(9) | 0.630(12) | 0.198(4) | 0.07(2) |

*Notes:* All atoms except for Pb were refined with isotropic displacement parameters. [a]$U_{eq}$ defined as one third of the trace of the orthogonalized $U_{ij}$ tensor. The coordinates of the $P2_1/c$ model have been reported without the ¼, ¼, ¼ origin shift to compare our data with those of other feldspar structures. The symmetry operators for this non-standard setting must be changed accordingly.

Table 5. Pb-O interatomic distances (Å)

| *P* (GPa) | 0.0001 | 2.4 | 3.1 | 5.4 | 6.0 | 7.2 |
|---|---|---|---|---|---|---|
| Space group | *I*2/*c* | *I*2/*c* | *I*2/*c* | *I*2/*c* | *I*2/*c* | *I*2/*c* |
| Pb-OA(1) | 2.65(2) | 2.63(3) | 2.65(5) | 2.53(3) | 2.51(4) | 2.75(6) |
| Pb-OA(1) | 2.76(2) | 2.81(3) | 2.78(5) | 2.84(3) | 2.83(4) | 2.67(6) |
| Pb-OA(2) | 2.48(1) | 2.44(1) | 2.44(2) | 2.38(3) | 2.41(3) | 2.23(6) |
| Pb-OB(0) | 2.87(2) | 2.76(4) | 2.66(3) | 3.02(5) | 3.11(7) | 3.00(14) |
| Pb-OB(z) | 3.02(3) | 2.99(4) | 3.00(8) | 2.60(3) | 2.55(4) | 2.49(4) |
| Pb-OC(0) | 3.17(4) | 3.21(4) | 3.35(6) | 3.06(4) | 3.02(5) | 3.03(4) |
| Pb-OC(z) | 3.14(3) | 2.95(3) | 2.82(4) | 2.89(4) | 2.90(4) | 2.94(6) |
| Pb-OD(0) | 2.79(3) | 2.74(4) | 2.76(4) | 2.69(6) | 2.74(5) | 2.60(5) |
| Pb-OD(z) | 2.67(2) | 2.85(4) | 2.75(5) | 2.78(3) | 2.78(5) | 2.83(11) |
| < Pb-O > | 2.84 | 2.82 | 2.80 | 2.75 | 2.76 | 2.73 |

| *P* (GPa) | 8.4 | 9.7 | *P* (GPa) | 8.4 | 9.7 |
|---|---|---|---|---|---|
| Space group | $P2_1/c$ | $P2_1/c$ | Space group | $P2_1/c$ | $P2_1/c$ |
| Pb(0)-OA(10) | 2.64(5) | 2.58(7) | Pb(i)-OA(10) | 2.66(5) | 2.59(7) |
| Pb(0)-OA(1i) | 2.79(7) | 2.74(7) | Pb(i)-OA(1i) | 2.60(7) | 2.52(8) |
| Pb(0)-OA(20) | 2.55(3) | 2.46(5) | Pb(i)-OA(20) | 2.93(3) | 2.91(5) |
| Pb(0)-OA(2i) | 3.33(3) | 3.26(5) | Pb(i)-OA(2i) | 2.36(3) | 2.33(5) |
| Pb(0)-OB(0i) | 2.93(5) | 3.32(11) | Pb(i)-OB(00) | 2.68(13) | 2.81(14) |
| Pb(0)-OB(zi) | 2.66(6) | 2.74(8) | Pb(i)-OB(z0) | 2.62(4) | 2.45(8) |
| Pb(0)-OC(0i) | 2.89(7) | 2.92(8) | Pb(i)-OC(00) | 3.07(5) | 3.08(7) |
| Pb(0)-OC(zi) | 2.41(6) | 2.24(8) | Pb(i)-OC(z0) | 2.94(5) | 2.98(7) |
| Pb(0)-OD(00) | 2.70(5) | 2.62(6) | Pb(i)-OD(0i) | 3.02(9) | 3.42(10) |
| Pb(0)-OD(z0) | 2.55(7) | 3.11(16) | Pb(i)-OD(zi) | 3.03(6) | 2.76(10) |
| < Pb-O > | 2.75 | 2.80 | < Pb-O > | 2.79 | 2.78 |

Table 6. T-O-T angles (°)

| *P* (GPa) | 0.0001 | 2.4 | 3.1 | 5.4 | 6.0 | 7.2 | | 8.4 | 9.7 |
|---|---|---|---|---|---|---|---|---|---|
| Space group | *I*2/*c* | *I*2/*c* | *I*2/*c* | *I*2/*c* | *I*2/*c* | *I*2/*c* | | $P2_1/c$ | $P2_1/c$ |
| T1(0)-OA(1)-T1(z) | 139(2) | 143(2) | 145(4) | 138(2) | 138(3) | 150(6) | T1(00)-OA(10)-T1(zi) | 130(4) | 120(5) |
| | | | | | | | T1(z0)-OA(1i)-T1(0i) | 150(7) | 150(7) |
| T2(0)-OA(2)-T2(z) | 130(1) | 130(1) | 132(2) | 131(2) | 134(2) | 122(4) | T2(00)-OA(20)-T2(z0) | 128(3) | 122(3) |
| | | | | | | | T2(zi)-OA(2i)-T2(0i) | 128(2) | 126(3) |
| T2(0)-OB(0)-T1(0) | 145(2) | 139(3) | 132(3) | 142(2) | 141(3) | 153(4) | T1(00)-OB(00)-T2(00) | 119(3) | 130(4) |
| | | | | | | | T1(0i)-OB(0i)-T2(0i) | 156(3) | 135(8) |
| T1(z)-OB(z)-T2(z) | 150(1) | 148(1) | 147(3) | 120(3) | 121(3) | 114(3) | T1(z0)-OB(z0)-T2(z0) | 133(4) | 117(6) |
| | | | | | | | T1(zi)-OB(zi)-T2(zi) | 132(3) | 137(5) |
| T1(0)-OC(0)-T2(0) | 131(2) | 127(2) | 133(4) | 123(2) | 117(3) | 124(2) | T1(00)-OC(00)-T2(0i) | 119(2) | 114(3) |
| | | | | | | | T1(0i)-OC(0i)-T2(00) | 125(4) | 122(4) |
| T1(z)-OC(z)-T2(z) | 132(1) | 130(2) | 122(2) | 124(2) | 131(3) | 132(4) | T1(z0)-OC(z0)-T2(zi) | 117(3) | 122(3) |
| | | | | | | | T1(zi)-OC(zi)-T2(z0) | 110(4) | 107(5) |
| T2(0)-OD(0)-T1(0) | 140(2) | 140(2) | 139(4) | 141(5) | 136(4) | 136(4) | T1(00)-OD(00)-T2(0i) | 137(4) | 134(6) |
| | | | | | | | T1(0i)-OD(0i)-T2(00) | 139(5) | 129(6) |
| T1(z)-OD(z)-T2(z) | 138(2) | 148(2) | 139(2) | 142(2) | 141(2) | 141(4) | T1(z0)-OD(z0)-T2(zi) | 133(5) | 127(6) |
| | | | | | | | T1(zi)-OD(zi)-T2(z0) | 162(3) | 151(8) |

Table 7. Number of *a*, *b*, *c* and *d* reflections and $I/\sigma(I)$ ratios for lead feldspar and monoclinic $An_{20}SrFsp_{80}$ feldspar[a] at different pressures

| | *P* (GPa) | Space group | No. refl. $I/\sigma(I) > 1$ | $\frac{\text{No. refl. } x}{\text{No. refl. } a}$ | $I/\sigma(I)$ mean | $I/\sigma(I)$ max |
|---|---|---|---|---|---|---|
| $PbAl_2Si_2O_8$ | 0.0001[b] | *I*2/*c* | | | | |
| *a* refl. | | | 389 | 1.0 | 23.5 | 121.0 |
| *b* refl. | | | 243 | 0.62 | 2.9 | 14.9 |
| total | | | 632 | - | - | - |
| $PbAl_2Si_2O_8$ | 7.2 | *I*2/*c* | | | | |
| *a* refl. | | | 258 | 1.0 | 12.7 | 110.1 |
| *b* refl. | | | 176 | 0.68 | 4.2 | 8.9 |
| total | | | 434 | - | - | - |
| $PbAl_2Si_2O_8$ | 8.4 | $P2_1/c$ | | | | |
| *a* refl. | | | 370 | 1.0 | 9.7 | 54.4 |
| *b* refl. | | | 181 | 0.49 | 2.2 | 8.3 |
| *c* refl. | | | 201 | 0.54 | 2.0 | 6.5 |
| *d* refl. | | | 342 | 0.92 | 5.0 | 21.0 |
| total | | | 1094 | - | - | - |
| $Ca_{0.2}Sr_{0.8}Al_2Si_2O_8$ | 4.4 | *I*2/*c* | | | | |
| *a* refl. | | | 226 | 1.0 | 24.2 | 85.1 |
| *b* refl. | | | 83 | 0.37 | 4.7 | 28.6 |
| total | | | 309 | - | - | - |
| $Ca_{0.2}Sr_{0.8}Al_2Si_2O_8$ | 7.4 | $P2_1/c$ | | | | |
| *a* refl. | | | 242 | 1.0 | 24.0 | 71.8 |
| *b* refl. | | | 150 | 0.62 | 6.5 | 46.4 |
| *c* refl. | | | 114 | 0.47 | 5.0 | 25.2 |
| *d* refl. | | | 241 | 1.0 | 13.6 | 57.0 |
| total | | | 747 | - | - | - |

*Note*: [a] Benna et al. (2007). [b] Within the DAC.

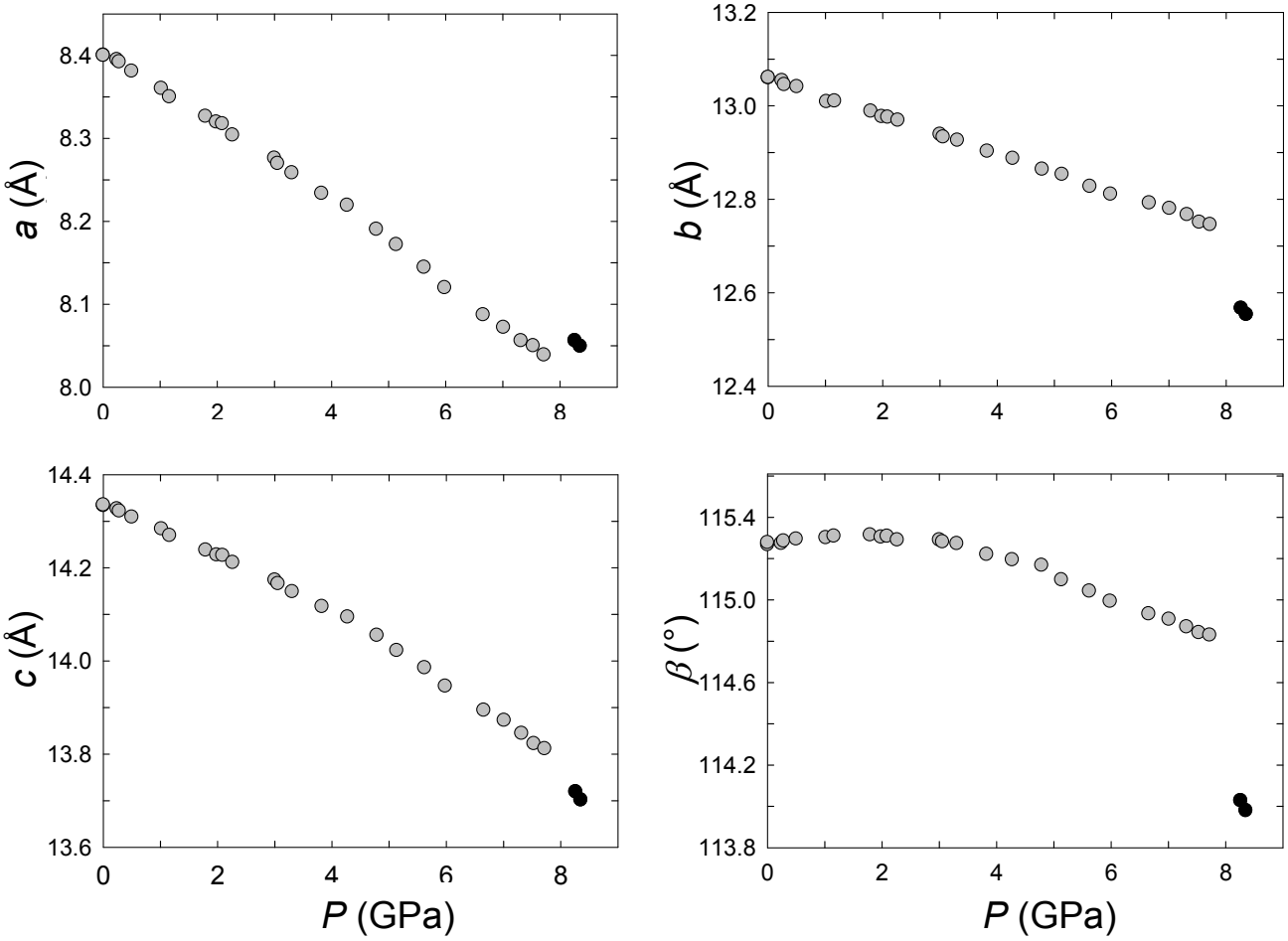


Figure 1

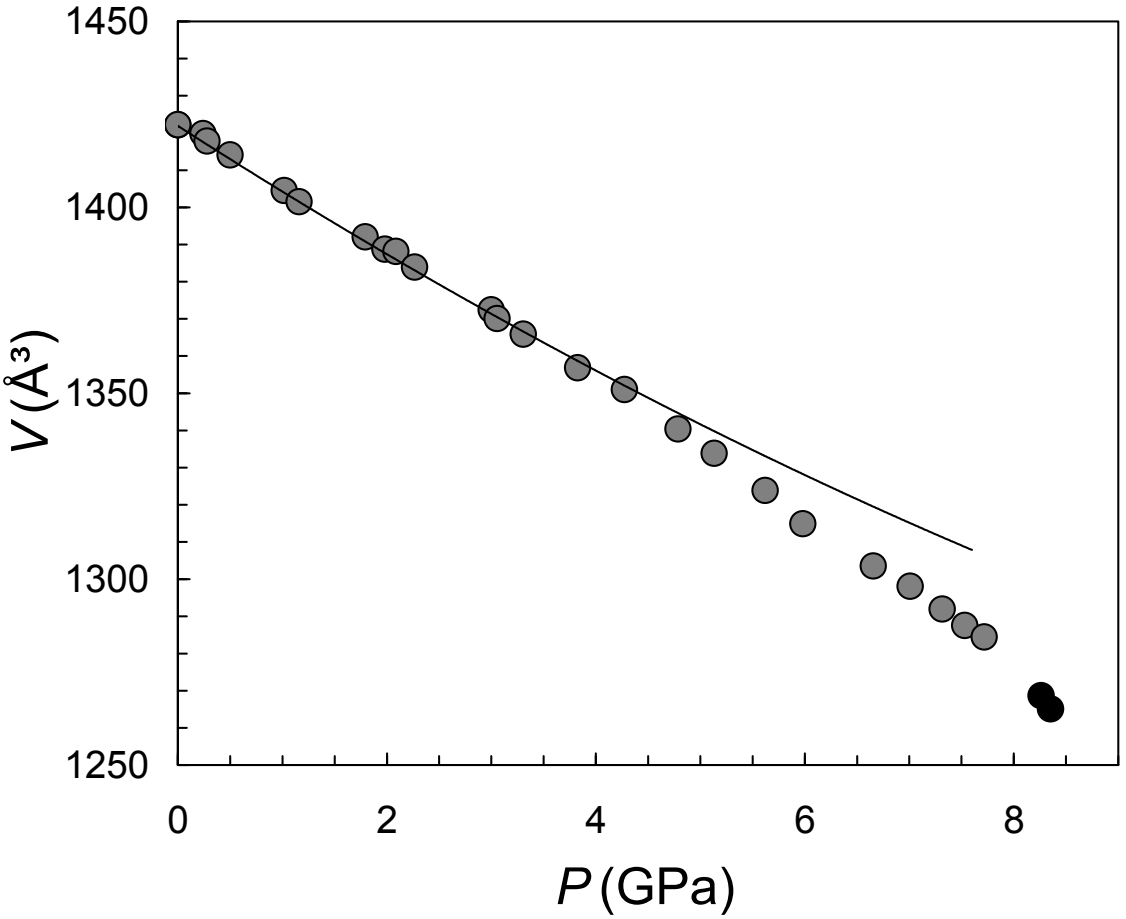


Figure 2

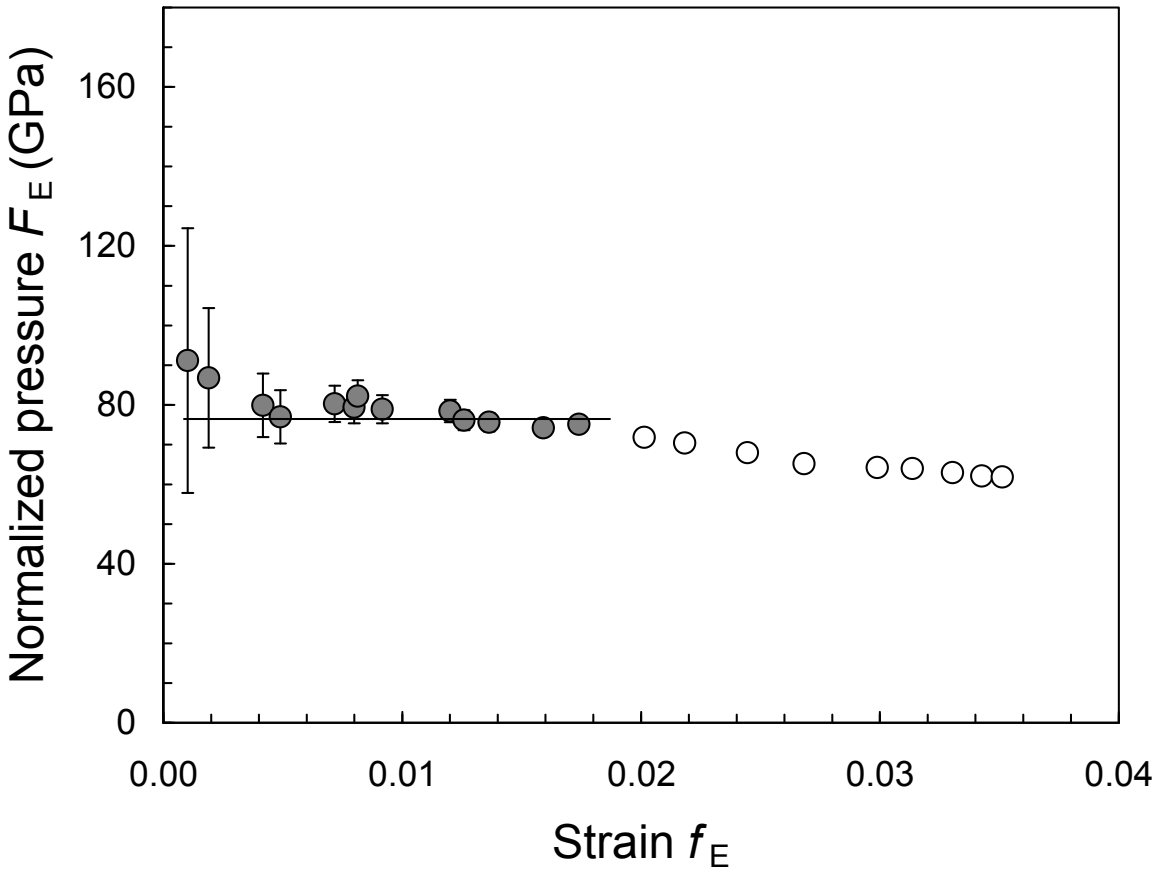
Normalized pressure $F_E$ (GPa)
160
120
80
40
0
0.00
0.01
0.02
0.03
0.04
Strain $f_E$

Figure 3

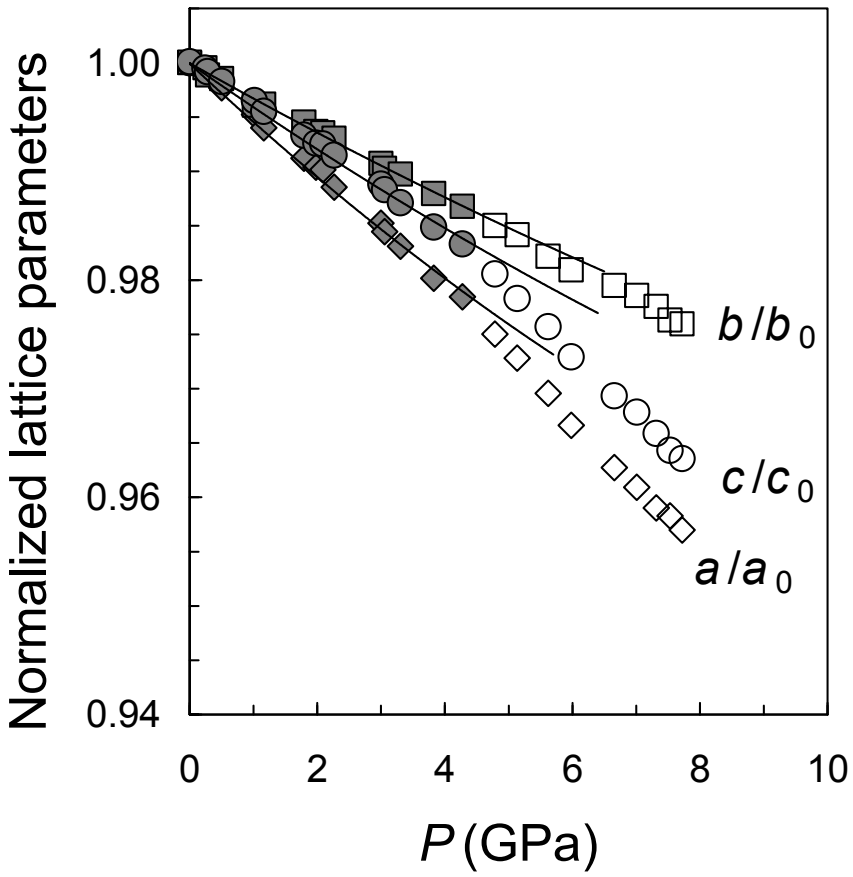
Normalized lattice parameters
1.00
0.98
0.96
0.94
0
2
4
6
8
10
P (GPa)
b/b0
c/c0
a/a0

Figure 4

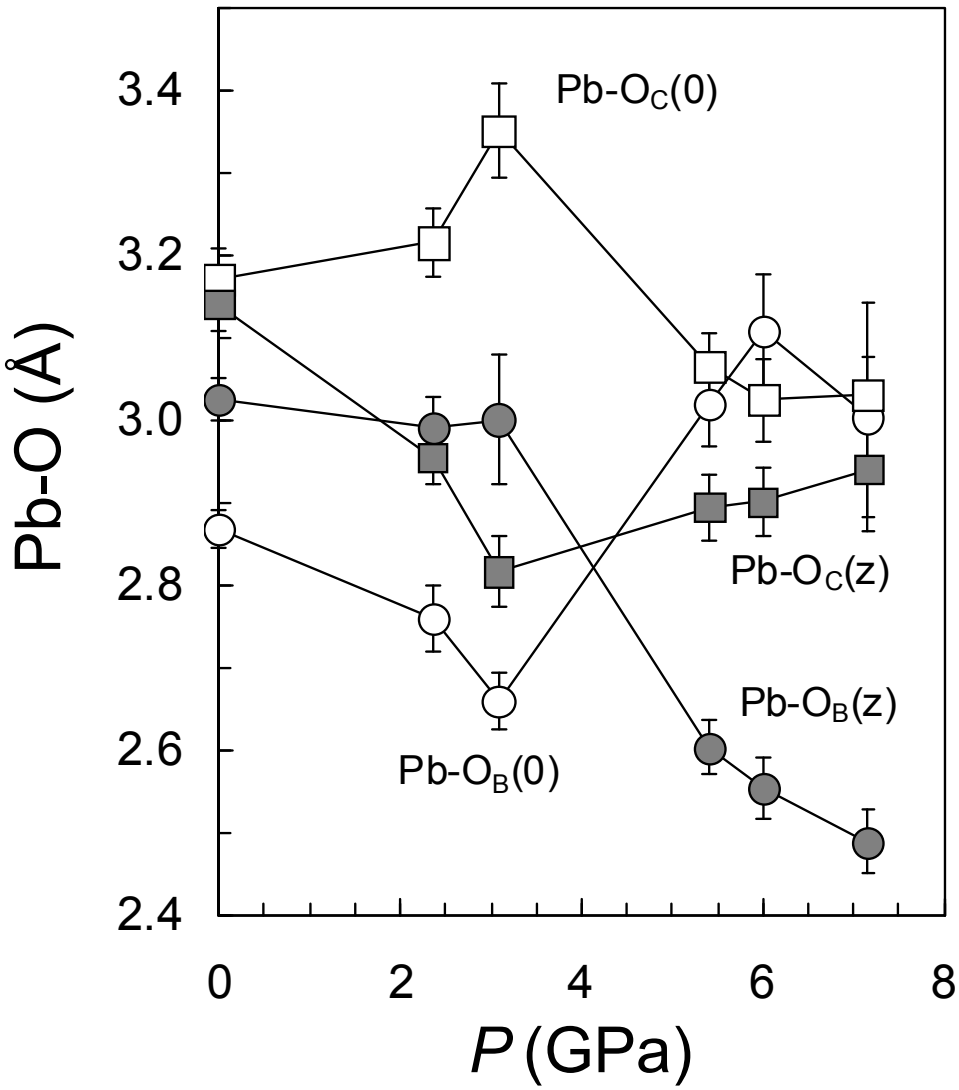


Figure 5

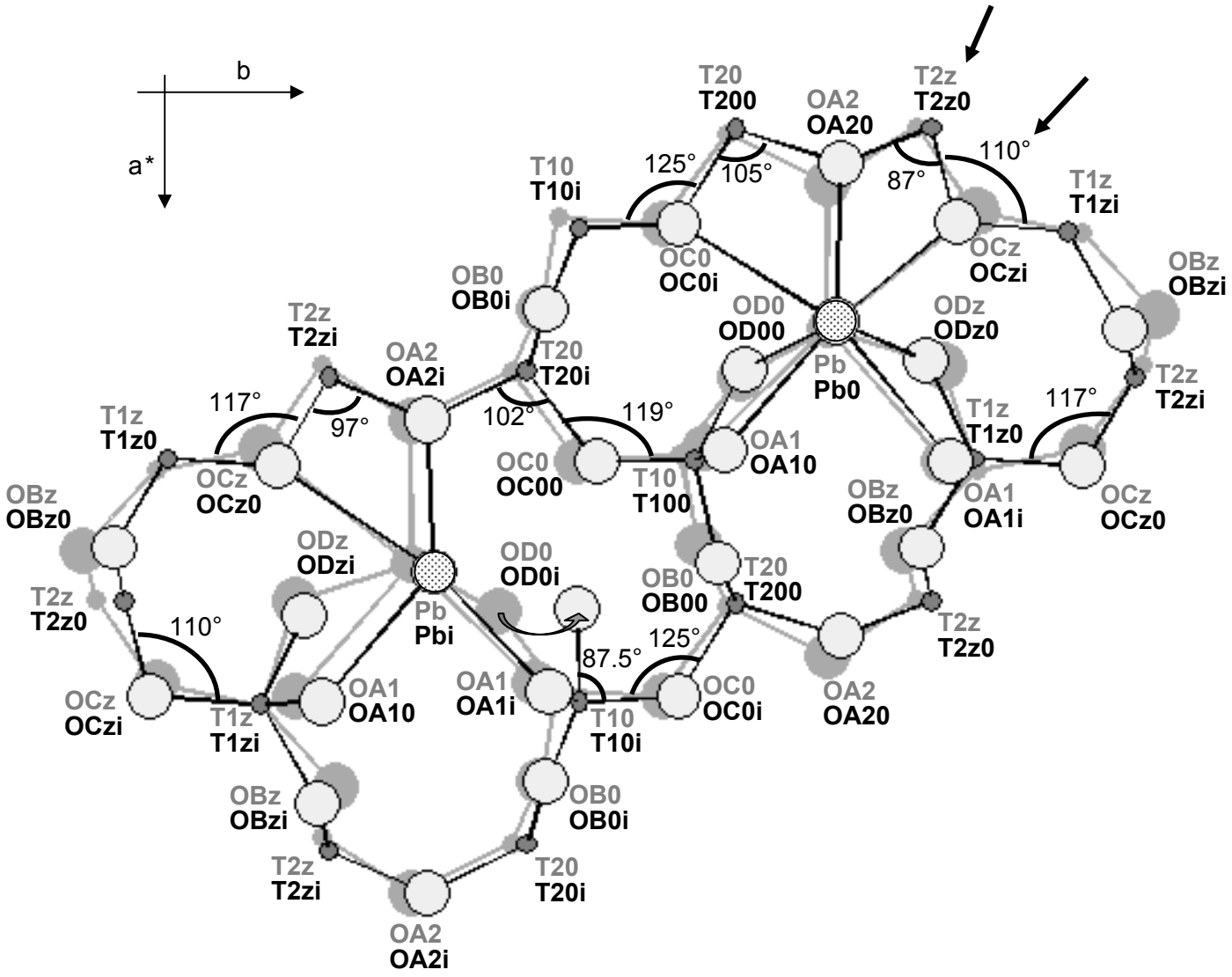
b
a*
T20
T200
OA2
OA20
T2z
T2z0
110°
125°
105°
87°
T10
T10i
T1z
T1zi
OC0
OC0i
OCz
OCzi
OBz
OBzi
OB0
OB0i
OD0
OD00
ODz
ODz0
T2z
T2zi
OA2
OA2i
T20
T20i
Pb
Pb0
117°
97°
102°
119°
T1z
T1z0
OA1
OA10
OC0
OC00
T10
T100
OBz
OBz0
OA1
OA1i
OCz
OCz0
ODz
ODzi
OD0
OD0i
OB0
OB00
T20
T200
T2z
T2z0
Pb
Pbi
87.5°
125°
110°
OCz
OCzi
OA1
OA10
OA1
OA1i
OC0
OC0i
OA2
OA20
T1z
T1zi
T10
T10i
OBz
OBzi
OB0
OB0i
T2z
T2zi
T20
T20i
OA2
OA2i

Figure 6

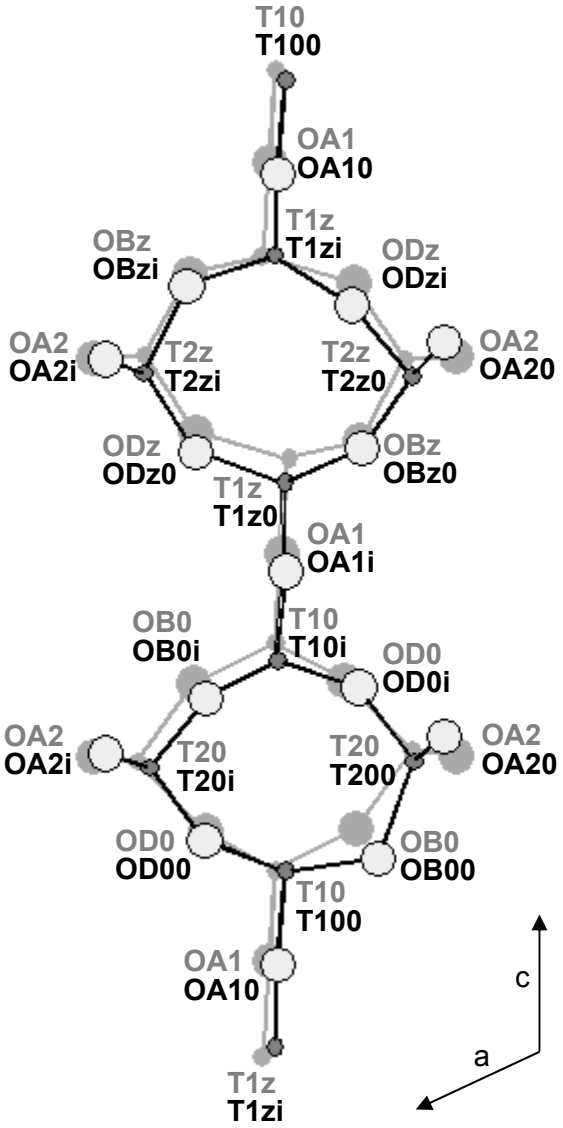
T10
T100
OA1
OA10
T1z
T1zi
OBz
OBzi
ODz
ODzi
OA2
OA2i
T2z
T2zi
T2z
T2z0
OA2
OA20
ODz
ODz0
OBz
OBz0
T1z
T1z0
OA1
OA1i
OB0
OB0i
T10
T10i
OD0
OD0i
OA2
OA2i
T20
T20i
T20
T200
OA2
OA20
OD0
OD00
OB0
OB00
T10
T100
OA1
OA10
T1z
T1zi
c
a

Figure 7